1-2014

Identification of an L-Phenylalanine Binding Site Enhancing The Cooperative Responses of The Calcium Sensing Receptor to Calcium

Chen Zhang
Georgia State University, czhang5@gsu.edu

Yun Huang
Georgia State University

Yusheng Jiang
Georgia State University

Nagaraju Mulpuri
Georgia State University, mulpurinagaraju@gsu.edu

Ling Wei
Georgia State University

See next page for additional authors

Follow this and additional works at: http://scholarworks.gsu.edu/chemistry_facpub

Part of the Chemistry Commons

Authors

Chen Zhang, Yun Huang, Yusheng Jiang, Nagaraju Mulpuri, Ling Wei, Donald Hamelberg, Edward M. Brown, and Jenny J. Yang

Identification of an L-Phenylalanine Binding Site Enhancing The Cooperative Responses of The Calcium Sensing Receptor to Calcium*

Chen Zhang[1], Yun Huang[1], Yusheng Jiang[1], Nagaraju Mulpuri[1], Ling Wei[1], Donald Hamelberg[1], Edward M. Brown[2], and Jenny J. Yang[1]

[1]Department of Chemistry, Center for Diagnostics and Therapeutics, Georgia State University, Atlanta, Georgia 30303;
[2]Division of Endocrinology, Diabetes and Hypertension, Department of Medicine, Brigham and Women's Hospital, Boston, MA 02115

*Running title: L-Phe and Ca^{2+} promote functional positive cooperativity of CaSR

To whom correspondence should be addressed: Jenny J. Yang, Department of Chemistry, Georgia State University, University Plaza, Atlanta, Georgia 30303 USA, Tel: 404-413-5520, Fax: 404-413-5551

Background : The Calcium-Sensing Receptor (CaSR) is a key mediator of Ca^{2+} homeostasis *in vivo*.
Results: An L-Phe binding site at the CaSR's hinge region globally enhances its cooperative activation by Ca^{2+}.
Conclusion: Communication between the binding sites for Ca^{2+} and L-Phe is crucial for functional cooperativity of CaSR-mediated signaling.
Significance: The results provide important insights into the molecular basis of Ca^{2+}-sensing by the CaSR.

Abstract

Functional positive cooperative activation of the extracellular calcium ($[Ca^{2+}]_o$)-sensing receptor (CaSR), a member of the family C G protein-coupled receptors (GPCRs), by $[Ca^{2+}]_o$ or amino acids elicits intracellular Ca^{2+} ($[Ca^{2+}]_i$) oscillations. Here, we report the central role of predicted Ca^{2+}-binding Site 1 within the hinge region of the extracellular domain (ECD) of CaSR and its interaction with other Ca^{2+}-binding sites within the ECD in tuning functional positive homotropic cooperativity caused by changes in $[Ca^{2+}]_o$. Next, we identify an adjacent L-Phe-binding pocket that is responsible for positive heterotropic cooperativity between $[Ca^{2+}]_o$ and L-Phe in eliciting CaSR-mediated $[Ca^{2+}]_i$ oscillations. The hetero-communication between Ca^{2+} and an amino acid globally enhances functional positive homotropic cooperative activation of CaSR in response to $[Ca^{2+}]_o$ signaling by positively impacting multiple $[Ca^{2+}]_o$-binding sites within the ECD. Elucidation of the underlying mechanism provides important insights into the longstanding question of how the receptor transduces signals initiated by $[Ca^{2+}]_o$ and amino acids into intracellular signaling events.

Introduction

It has long been recognized that Ca^{2+} acts as a second messenger that is released from intracellular stores and/or taken up from the extracellular environment in response to external stimuli to regulate diverse cellular processes. The discovery of the parathyroid Ca^{2+}-sensing receptor (CaSR) by Brown *et al.* has established a new paradigm of Ca^{2+} signaling (1). In addition to its known role as a second messenger, extracellular Ca^{2+} can function as a first messenger by CaSR-mediated triggering of multiple intracellular signaling pathways, including activation of phospholipases C, A_2, and D, and various mitogen-activated protein kinases (MAPKs), as well as inhibition of cAMP production (2-7). This

1

receptor is present in the key tissues involved in [Ca^{2+}]$_o$ homeostasis (e.g., parathyroid, kidney, bone) and diverse other non-homeostatic tissues (e.g., brain, skin, etc.) (8-11). CaSR consists of a large N-terminal extracellular domain (ECD) (~600 residues) folded into a Venus Fly Trap (VFT) motif, followed by a 7-pass transmembrane region (7TM) and a cytosolic C-terminus. The ECD has been shown to play an important role in the cooperative response of the CaSR to [Ca^{2+}]$_o$. Elevations in [Ca^{2+}]$_o$ activate the CaSR, evoking increases in the intracellular Ca^{2+} concentration ([Ca^{2+}]$_i$), producing [Ca^{2+}]$_i$ oscillations, modulating the rate of parathyroid hormone (PTH) secretion, and regulating gene expression (3,12-14). The pattern of [Ca^{2+}]$_i$ oscillations is one of the most important signatures reflecting the state of CaSR activity.

More than two hundred naturally-occurring mutations have been identified in the CaSR that either inactivate the receptor (reducing sensitivity to [Ca^{2+}]$_o$), leading to familial hypocalciuric hypercalcemia (FHH) or neonatal severe hyperparathyroidism (NSHPT), or activate it (increasing sensitivity to [Ca^{2+}]$_o$), thereby causing autosomal dominant hypoparathyroidism (ADH) (15-17). Several of these naturally-occurring mutations of CaSR exhibit altered functional cooperativity (15).

Functional cooperativity of CaSR (i.e., based on biological activity determined using functional assays rather than a direct binding assay), particularly the functional positive homotropic cooperative response to [Ca^{2+}]$_o$, is essential for the receptor's ability to respond over a narrow physiological range of [Ca^{2+}]$_o$ (1.1-1.3 mM) (3). CaSR has an estimated Hill coefficient of 3-4 for its regulation of processes such as activating intracellular Ca^{2+} signaling and inhibiting PTH release. Under physiological conditions, L-amino acids, especially aromatic amino acids (e.g., L-Phe), as well as short aliphatic and small polar amino acids (18), potentiate the high [Ca^{2+}]$_o$–elicited activation of the CaSR by altering the EC$_{50}$ values required for [Ca^{2+}]$_o$-evoked [Ca^{2+}]$_i$ responses and its functional cooperativity (19,20). In aggregate, the levels of amino acids in human serum in the fed state are close to those activating the CaSR *in vitro* (19,21) and can further enhance functional cooperativity via positive heterotropic cooperativity. Recently, several groups have reported that the CaSR in cells within the lumen of the gastrointestinal (GI) tract is activated by L-Phe and other amino acids, which have long been recognized as activators of key digestive processes. Hence, the CaSR enables the GI tract to monitor events relevant to both mineral ion and protein/amino acid metabolism in addition to the CaSR's sensing capability in blood and other extracellular fluids (19,22,23). Glutathione and its γ-glutamylpeptides also allosterically modulate the CaSR at a site similar to the L-amino acid-binding pocket but with over 1,000-fold higher potencies (20,24). Thus, CaSR is essential for monitoring and integrating information from both mineral ions/nutrients/polyamines in blood and related extracellular fluids. Nevertheless, we still lack a thorough understanding of the molecular mechanisms by which CaSR is activated by [Ca^{2+}]$_o$ and amino acids, which, in turn, regulate CaSR functional positive cooperativity. In addition, in a clinical setting, the molecular basis for the alterations in this cooperativity caused by disease-associated mutations is largely unknown due to the lack of knowledge of this receptor's structure and its weak binding affinities for [Ca^{2+}]$_o$ and amino acids (13,15,25,26).

In the present study, we use two complementary approaches--monitoring [Ca^{2+}]$_i$ oscillations in living cells and performing molecular dynamic (MD) simulations--to provide important insights into how the CaSR functions and the behavior of the receptor at the atomic level. We first demonstrate that the molecular connectivity between [Ca^{2+}]$_o$–binding sites that is encoded within the key Ca^{2+}-binding Site 1 in the hinge region of the CaSR's ECD is responsible for the functional positive homotropic cooperativity in the CaSR's response to [Ca^{2+}]$_o$. We further identify an L-Phe-binding pocket adjacent to Ca^{2+}-binding Site 1. We show that occupancy of this binding pocket by L-Phe is essential for functional positive heterotropic cooperativity by virtue of its having a marked impact on all five of the predicted Ca^{2+}-binding sites in the ECD with

2

regard to $[Ca^{2+}]_o$-evoked $[Ca^{2+}]_i$ signaling. Furthermore, with MD simulations we show that the simulated motions of Ca^{2+}-binding Site 1 are correlated with those of the other predicted Ca^{2+}-binding sites. Finally, the dynamic communication of L-Phe at its predicted binding site in the hinge region with the CaSR's Ca^{2+}–binding sites not only influences the adjacent $[Ca^{2+}]_o$ binding site 1 but globally (i.e., by exerting effects widely over the ECD) enhances cooperative activation of the receptor in response to alterations in $[Ca^{2+}]_o$.

Material and Methods

Computational Prediction of L-Phe-binding Site and Ca^{2+}-Binding Sites from a Model Structure. The structure of the extracellular domain of CaSR (residues 25-530) was modeled based on the crystal structure of mGluR1 (1EWT, 1EWK and 1ISR), and the potential Ca^{2+}-binding sites in the CaSR ECD were predicted using MetalFinder (25,27). Prediction of the L-Phe-binding site was performed by AutoDock-Vina (28). In brief, the docking center and grid box of the model structure and the rotatable bonds of L-Phe were defined by AutoDock tools-1.5.4. The resultant L-Phe coordinates were combined back to the pdb file of the model structure for input into the LPC/CSU server to analyze interatomic contacts between the ligand and receptor (29). The residues within 5 Å around L-Phe were considered as L-Phe-binding residues.

Measurement of $[Ca^{2+}]_i$ responses in single cells transfected with WT or mutant CaSRs with or without L-Phenylalanine. Measurement of intracellular free Ca^{2+} was assessed as described by Huang, et al. (30). Briefly, wild type CaSR or its mutants were transiently transfected into HEK293 cells grown on coverslips and cultured for 48 h. The cells were subsequently loaded for 15 min using 4 µM Fura-2 AM in 2 mL physiological saline buffer (10 mM HEPES, 140 mM NaCl, 5 mM KCl, 1.0 mM MgCl$_2$, 1 mM CaCl$_2$ and pH 7.4). The coverslips were mounted in a bath chamber on the stage of a Leica DM6000 fluorescence microscope, and the cells were incubated in calcium-free physiological saline

buffer for 5 mins. The cells were then alternately illuminated with 340 or 380 nm light, and the fluorescence at an emission wavelength 510 nm was recorded in real time as the concentration of extracellular Ca^{2+} was increased in a stepwise manner in the presence or absence of 5 mM L-Phe. The ratio of the emitted fluorescence intensities resulting from excitation at both wavelengths was utilized as a surrogate for changes in $[Ca^{2+}]_i$ and was further plotted and analyzed as a function of $[Ca^{2+}]_o$. All experiments were performed at room temperature. The signals from 30 to 60 single cells were recorded for each measurement. Oscillations were defined as three successive fluctuations in $[Ca^{2+}]_i$ after the initial peak.

Measurement of $[Ca^{2+}]_i$ in cell populations by fluorimetry. The $[Ca^{2+}]_i$ responses of wild type CaSR and its mutants were measured as described by Huang, et al. (25). Briefly, CaSR-transfected HEK293 cells were grown on 13.5 × 20 mm coverslips. After the cells reached 90% confluence, they were loaded by incubation with 4 µM Fura-2 AM in 20 mM HEPES, containing 125 mM NaCl, 5 mM KCl, 1.25 mM CaCl$_2$, 1 mM MgCl$_2$, 1 mM NaH$_2$PO4, 1% glucose, and 1% BSA (pH 7.4) for 1 h at 37° and then washed once with 20 mM HEPES, pH 7.4, containing 125 mM NaCl, 5 mM KCl, 0.5 mM CaCl$_2$, 0.5 mM MgCl$_2$, 1% glucose, and 1% BSA (bath buffer). The coverslips with transfected, Fura-2-loaded HEK293 cells were placed diagonally in 3-ml quartz cuvettes containing bath buffer. The fluorescence spectra at 510 nm were measured during stepwise increases in $[Ca^{2+}]_o$ with alternating excitation at 340 or 380 nm. The ratio of the intensities of the emitted light at 510 nm when excited at 340 or 380 nm was used to monitor changes in $[Ca^{2+}]_i$. The EC$_{50}$ and Hill constants were fitted using the Hill equation

$$\Delta S = \frac{[M]^n}{K_d^{\ n} + [M]^n}$$ where ΔS is the total signal change in the equation.

MD simulation and correlation analysis using Amber. MD simulation provides an approach complementary to the experiments in live cells for understanding biomolecular structure, dynamics,

and function. The initial coordinates for all the simulations were modeled from the 2.20 Å resolution x-ray crystal structure of mGluR1 with PDBID 1EWK (31). The AMBER 10 suite of programs (32) was used to carry out all of the simulations in an explicit TIP3P water model (33), using the modified version of the all-atom Cornell et. al. (34) force field and the re-optimized dihedral parameters for the peptide ω-bond (35). An initial 2 ns simulation was performed using NOE restraint during the equilibration in order to reorient the side chains residues in the Ca^{2+}-binding site, but no restraints were used during the actual simulation. A total of three MD simulations were carried out for 50 ns each on the apo-form and ligand loaded forms. During the simulations, an integration time step of 0.002 ps was used to solve Newton's equation of motion. The long-range electrostatic interactions were calculated using the Particle Mesh Ewald method, (36) and a cutoff of 9.0 Å was applied for non-bonded interactions. All bonds involving hydrogen atoms were restrained using the SHAKE algorithm (37). The simulations were carried out at a temperature of 300 K and a pressure of 1 bar. A Langevin thermostat was used to regulate the temperature with a collision frequency of 1.0 ps-1. The trajectories were saved every 500 steps (1ps). The trajectories were analyzed using the ptraj module in Amber 10.

Accelerated Molecular Dynamics Simulation. Accelerated MD (aMD) was carried out on the free CaSR ECD using the RaMD method (38) implemented in a pmemd module of AMBER on the rotatable torsion. A boost energy, E, of 2000kcal/mol was added to the average dihedral energy and a tuning parameter, α, of 200 kcal/mol was used. The dual boost was also applied to accelerate the diffusive and solvent dynamics as previously described (39). The simulation conditions were similar to that of the normal MD simulations above. Principal Component Analysis was carried out on the trajectories using the ptraj module in AMBER. The directions of the eigenvectors for the slowest modes were visualized using the Interactive Essential Dynamics (IED) plugin (40).

Docking Studies of Phe, Asp, and GLUT. The binding energies for the ligands were calculated using an ensemble-docking method and Autodock vina (28). The ensemble of conformations of CaSR was generated using molecular dynamics simulations as described above. Gasteiger charges were assigned to the ligands and CaSR using the Autodock ADT program. The ligands were flexible during docking to each conformation of CaSR using the following parameters: the grid spacing was 1.0 Å; the box size was 25 Å in each dimension, and the center of the box was chosen as the center of the active site of CaSR, with a large enough space to sample all possible ligand conformations within the box. The maximum number of binding modes saved was set to 10. The conformation with the lowest binding energy was used and assumed to be the best binder. Distributions of the binding energies for each ligand were calculated based on the lowest binding energy of each ligand to each conformation in the ensemble of CaSR conformations.

Principal Component Analysis (PCA). Using the ptraj module of AMBER 10, the Principal Component Analysis (41,42) was performed on all the atoms of the residues that are 5 Å away from Site 1 of CaSR ECD. The covariance matrix of the x, y, and z coordinates of all the atoms obtained from each snapshot of the combined trajectories of the ligand-free CaSR ECD, the Ca^{2+}-loaded form, the form loaded with only L-Phe, and the form loaded with both Ca^{2+} and L-Phe were calculated. The covariance matrix was further diagonalized to produce orthonormal eigenvectors and their corresponding eigenvalues, ranked on the basis of their corresponding variances. The first three eigenvectors, the Principal Components, which contributed the majority of all the atomic fluctuations, were used to project the conformational space onto them, i.e., along two dimensions.

Statistics. The data are presented as means ± SE for the indicated number of experiments. Statistical analyses were carried out using the unpaired Student's t-test when two groups were compared. A P value of < 0.05 was considered to indicate a statistically significant difference.

4

Results
Molecular connectivity among predicted calcium-binding sites is required for functional positive cooperativity of CaSR

It has been documented that in several regions of the CaSR and mGluRs the amino acid residues are highly conserved (43). Those conserved elements provide a structural framework for the modeling of the CaSR ECD. Among all the available crystal structures of the mGluRs, studies on mGluR1 give concrete structural information about ligand-free as well as various ligand-bound forms of the receptor. Moreover, CaSR and mGluR1 share similar signaling pathways and can form heterodimers with one another either *in vivo* or *in vitro* (44). Thus, the crystal structures of mGluR1 were employed for modeling the CaSR ECD. By using our own computational algorithms, we previously identified five putative Ca^{2+}-binding sites in the modeled CaSR ECD (Fig. 1) (25,26,45). Among these, Site 1 is located in the hinge region between the two lobes in the VFT motif. Among 34 newly identified naturally-occurring missense mutations within the ECD, 18 are located within 10 Å of one or more of the predicted Ca^{2+}-binding sites (15). Interestingly, a few disease-associated human mutations severely impair the functional cooperativity of CaSR (46) .

Functional positive homotropic cooperativity here refers to [Ca^{2+}]$_o$-induced changes in CaSR activity that can be ascribed to interactions between the five predicted Ca^{2+}-binding sites, which are located in different regions of the ECD (47-49). To understand the observed cooperativity and the origin of changes in cooperativity caused by disease-associated mutations at the atomic level, we have carried out MD simulations on the modeled CaSR ECD to predict correlated motions. MD simulation provides an approach complementary to the experiments in live cells for understanding biomolecular structure, dynamics, and function (50). We calculated the cross-correlation coefficients of each residue with those of all of the other residues in the CaSR ECD from the simulations (Material and Methods). Fig. 1 (lower-right panel) shows the normalized correlation matrix map of both negative (blue) and positive (red) correlated motions between each pair of residues. Negative and positive correlated motions indicate movements in the opposite direction or in the same direction, respectively. Positive correlations occur between groups of residues if they are within the same domain or directly interact with each other. Fig. 1 shows strong correlations amongst residues from S169 to A324. Notably, the negative correlated motions between residues K47-L125 and residues S240-A300 suggest that the two lobes undergo a dynamic change similar to that of mGluR1 upon interactions with its ligands. Closer analysis indicates that residues involved in Ca^{2+}-binding Site 1 exhibit negative correlations with residues in Sites 2, 3, 4 and 5 (Table 1).

We then predicted a putative amino acid-binding site in the modeled CaSR based on its sequence homology to mGluR1 and its ligand-loaded form using AutoDock-Vina (28). As shown in Fig. 1 (upper-left panel), this potential amino acid-binding pocket, formed by residues K47, L51, W70, T145, G146, S169, S170, I187, Y218, S272, H413 and R415, partially overlaps Ca^{2+}-binding Site 1 in the modeled CaSR ECD. Its predicted location is consistent with previous functional studies, suggesting important roles for S170 and T145 in amino acid-potentiated intracellular calcium responses (51-53). This L-Phe-binding site is also located within the hinge region of the ECD of CaSR with a relatively localized configuration during MD simulations. Other Ca^{2+}-binding Sites (Sites 2-5) are more than 10 Å away from the L-Phe-binding site (26). This partial colocalization of predicted Ca^{2+}-binding site 1 and the amino acid-binding site at the hinge domain in the ECD of the CaSR is also observed in other members of the family C GPCRs, including mGluRs and taste receptors, which share some degree of sequence similarity with the CaSR (Fig. 2a) (1,5,10,16,54-56). The calculated free energies for the binding of CaSR with various ligands (in the order of glutathione>L-Phe>L-Asp) is in excellent agreement with the experimental results

5

obtained by determining the EC$_{50}$ of intracellular Ca^{2+} responses to the same ligands (Fig. 2b) (19).

We define functional positive heterotropic cooperativity as that which occurs when the functional positive cooperative effect of interaction with one ligand (e.g., Ca^{2+}) affects the functional response resulting from interaction of a different ligand with the protein (i.e., an aromatic amino acid) (57). This term can be applied in the case of CaSR when it simultaneously senses Ca^{2+} and L-Phe. We have also observed greater correlated motions among the multiple Ca^{2+}-binding sites after docking both Ca^{2+} and L-Phe compared with docking of L-Phe alone to the ECD domain of the CaSR (Fig. 2c). Taking these results together, we propose that there is molecular connectivity centered at predicted calcium-binding Site 1 that plays an essential role in regulating the correlated motions among the multiple Ca^{2+}-binding sites. Further communication of this site with the amino acid-binding site is likely to mediate functional heterotropic cooperativity of CaSR-mediated signaling, as shown later.

Functional positive homotropic cooperativity among Ca^{2+}-binding sites.

Given that it is not readily possible to perform radioligand binding assays on CaSR due to its low affinities for its ligands, especially Ca^{2+} (e.g., mM K$_d$) as well as difficulty in purification of CaSR, we monitored intracellular calcium ([Ca^{2+}]$_i$) responses using both a cuvette population assay and by monitoring [Ca^{2+}]$_i$ oscillations using single cell imaging to determine functional cooperativity of CaSR. HEK293 cells transfected with WT CaSR exhibited sigmoidal concentration response curves for [Ca^{2+}]$_o$-evoked [Ca^{2+}]$_i$ responses (as monitored by changes in the ratio of fluorescence at 510 nm when excited at 340 or 380 nm) during stepwise increases in [Ca^{2+}]$_o$ with a Hill coefficient of 3.0 ± 0.1 and a EC$_{50}$ of 2.9 ± 0.2 mM. This result suggests strong positive homotropic cooperativity within the CaSR's five predicted Ca^{2+}-binding sites (Fig. 3). The sensitivity to agonist was assessed using the [Ca^{2+}]$_o$ at which cells began to show [Ca^{2+}]$_i$ oscillations and the frequency of the oscillations at the respective levels of [Ca^{2+}]$_o$ at which more than 50% of the cells started to oscillate.

To seek the key determinants underlying the observed functional positive homotropic cooperativity, mutations were introduced into the various predicted Ca^{2+}-binding sites of the CaSR by site-directed mutagenesis. The mutated receptors exhibited impaired Ca^{2+}-sensing capabilities with altered oscillation patterns in single cell studies and higher EC$_{50}$ values compared with WT CaSR in population studies (Tables 2 & 3, Figs. 3 & 4). Such population studies were also reported in our previous studies (25,26). Results from western blot and immunofluorescence staining using an anti-CaSR antibody indicated essentially equivalent expression of WT CaSR as well as its variants on the cell surface (Fig. 5). As shown in Fig. 3a, the level of [Ca^{2+}]$_o$ required to initiate oscillations in mutant E297I at predicted Ca^{2+}-binding Site 1 or D215I at Site 2 increased markedly from 3.0 ± 0.1 mM to 17.0 ± 0.4 mM and 13.9 ± 0.2 mM, respectively (n>30, p<0.05). Correlating well with these results, the two mutants had significantly impaired responses to [Ca^{2+}]$_o$ in the population assay with increased EC$_{50}$ values (Table 3). The Hill coefficients in Table 3 and Fig. 3b indicate that the cooperativity among the various Ca^{2+}-binding sites was impaired by mutating each of them separately. Strikingly, removal of Ca^{2+}-binding ligand residues, such as E297I and Y218Q at Site 1, converted the single process for functional activation of the WT CaSR by [Ca^{2+}]$_o$ to biphasic functional processes, suggesting that the underlying cooperative binding mechanism had been substantially perturbed (Figs. 3b & 6d).

Functional positive heterotropic cooperativity contributed by the identified L-Phe-binding site.

Fig. 6a shows the effect of 5 mM L-Phe on the [Ca^{2+}]$_i$ responses at different levels of [Ca^{2+}]$_o$ in HEK293 cells transiently transfected with the WT CaSR or its variants with mutations around the predicted L-Phe-sensing site. L-Phe lowered the threshold for [Ca^{2+}]$_o$–induced oscillations in the WT CaSR from 3.0 ± 0.1 mM to 2.0 ± 0.2 mM, a 1.5-fold decrease (Fig. 6a, Table 2). Concurrently, L-Phe also increased the oscillation frequency from 1.5 ± 0.1 to 2.2 ± 0.2 peaks/min (n>30, p<0.05) in the presence of 3.0

mM $[Ca^{2+}]_o$ in the single cell assay (Fig. 6c, Table 2). Meanwhile, L-Phe produced functional positive heterotropic cooperativity of the receptor, as it facilitated the response of the WT CaSR to $[Ca^{2+}]_o$ by significantly decreasing the EC_{50} from 2.9 ± 0.2 mM to 1.9 ± 0.2 mM (n=3, p<0.05) and increasing the Hill coefficient from 3.0 to 4.0 in the cell population assay (Fig. 6d, Table 3).

We then performed detailed analyses to understand the role of residues in the modeled L-Phe-binding site in the functional positive heterotropic cooperativity contributed by L-Phe (Fig. 6, and Table 4). Five out of 12 residues located within 5 Å of the modeled L-Phe-binding site exhibited impaired L-Phe-sensing ability. Mutants L51A and S170T exhibited impaired L-Phe-sensing capability as indicated by the absence of any change in the starting point (Fig. 6b) as well as constant oscillatory frequencies (~1.7 and 1.4 peaks/min) in the presence of L-Phe (Fig. 6c), while they maintained relatively unaltered calcium-sensing functions. Consistent with the single cell assay results, cell population studies revealed that the EC_{50} values of L51A, S170T and Y218Q remained the same with or without L-Phe (Fig. 6d) [the effect of L-Phe on S170T has previously been reported by Zhang et. al. in a cell population assay (51)]. Addition of 5 mM L-Phe lowered the $[Ca^{2+}]_o$ required to initiate oscillations in cells transfected with mutations S272A or T145A but failed to increase the oscillatory frequency at 2.5 mM $[Ca^{2+}]_o$ (the level at which the majority of the cells began to oscillate), nor did it reduce the EC_{50} (Table 4, Fig. 7). Y218 is predicted to be involved in binding of both L-Phe in its binding pocket and of Ca^{2+} in Site 1. Indeed, the mutation Y218Q largely disrupted the functional positive homotropic cooperativity with transformation of the single cooperative response to $[Ca^{2+}]_o$ of the WT CaSR to a biphasic process in the cell population assay. Y218Q also exhibited less sensitivity to $[Ca^{2+}]_o$, as $[Ca^{2+}]_i$ oscillations did not start until $[Ca^{2+}]_o$ was increased to more than 10 mM, reflecting its role in this Ca^{2+}-binding site. Of note, however, addition of 5 mM L-Phe failed to restore the calcium sensitivity of this mutant as manifested by an unchanged oscillation pattern. An oscillation frequency of ~1.5

peaks/min was observed at 20 mM $[Ca^{2+}]_o$ both with and without L-Phe for this mutant. In contrast, mutations such as K47A, Y63I, W70L, G146A, I162A, S169A, I187A, H413L, and R415A did not abrogate the positive allosteric effect of 5 mM L-Phe (Table 4). Taken together, these results suggest that residues located at the predicted L-Phe-binding site, including L51, T145, S170, S272, and Y218, play key roles in sensing L-Phe.

Global functional positive heterotropic cooperative tuning by L-Phe of the positive homotropic cooperative response of CaSR to $[Ca^{2+}]_o$

The sensing of L-Phe at the hinge region adjacent to Site 1 has marked global (i.e., extending widely over the ECD) effects on the five predicted Ca^{2+}-binding sites predicted earlier, which are spread over several different locations in the CaSR's ECD. Interestingly, addition of 5 mM L-Phe significantly rescued the $[Ca^{2+}]_i$ responses of the two mutants, E297I and D215I, in Sites 1 and 2, respectively, that exhibited disrupted cooperativity. Notably, L-Phe converted the biphasic Ca^{2+}-response curve for E297I back to a uniphasic curve (Fig. 8). Fig. 8 shows that their starting points for $[Ca^{2+}]_o$-initiated oscillations were reduced from 17.0 ± 0.4 mM to 7.3 ± 0.2 mM (E297I) and from 13.9 ± 0.2 mM to 6.7 ± 0.3 mM (D215I), respectively, in the presence of L-Phe (Table 2). Both of the mutants exhibited more than 2-fold-shifts in their starting points in the presence of L-Phe. The frequencies of their oscillations increased to more than 2 peaks/min in both cases compared to the frequencies without L-Phe (Fig. 8c and Table 2). Similarly, addition of L-Phe decreased their EC_{50}s in the cell population assay (Table 3).

Mutant E224I at Site 3 exhibited increases in the $[Ca^{2+}]_o$ required to initiate $[Ca^{2+}]_i$ oscillations but manifested smaller changes (from 3.0 ± 0.1 mM to 5.0 ± 0.2 mM $[Ca^{2+}]_o$ (n>30, P<0.05), compared with the previous two mutants. Moreover, its elevated EC_{50} value obtained in the population study correlated well with results from the single cell study (Tables 2&3) suggesting an impaired ability of this mutant to sense $[Ca^{2+}]_o$. But addition of L-Phe not only significantly

decreased the level of [Ca^{2+}]$_o$ required for initiating oscillations but also increased the oscillation frequency measured at the same level of [Ca^{2+}]$_o$. Furthermore, the population assay showed that the EC$_{50}$ was reduced and the maximum response was rescued by 5 mM L-Phe.

E353 is part of Ca^{2+}-binding Site 4 in lobe 2, while D398 and E399 are involved in Site 5 (26). Table 3 and Fig. 4 show that removal of these negatively charged residues at Sites 4 and 5 increased the level of [Ca^{2+}]$_o$ required to initiate [Ca^{2+}]$_i$ oscillations and also the mutant receptors' EC$_{50}$s. L-Phe at 5 mM was able to enhance these mutants' sensitivity to [Ca^{2+}]$_o$ and decrease their EC$_{50}$s. Therefore, as shown in Table 2, not only Ca^{2+}-binding residues adjacent to the predicted L-Phe-binding site (e.g., Sites 1 and 2) but also sites farther away from the hinge region exhibited L-Phe-induced decreases in EC$_{50}$ and starting point as well as increases in oscillation frequency and Hill coefficient.. This result suggests the global nature of the functional positive heterotropic cooperative interaction between L-Phe and extracellular Ca^{2+}.

The ensemble of conformations of calcium- and L-Phe-loaded CaSR ECD is distinguishable from the non-loaded forms.

To provide a more detailed description of the CaSR's mechanism of action at the atomic level, we again used MD simulations to analyze the trajectories of these simulations using principal component analysis (PCA) (Material & Methods), which separates out the protein motions into principal modes ranked according to their relative contributions (41). Projection of the trajectories of the different states of CaSR onto the first three modes, which accounted for the majority of the total fluctuations, is shown in Fig. 9a. The conformations sampled by the Ca^{2+}-free and L-Phe-free forms of the CaSR are distinctly different from those sampled by the Ca^{2+}-loaded and Ca^{2+}- and L-Phe-loaded forms of the receptor. Interestingly, the conformations of the L-Phe-loaded and the free form of CaSR are essentially indistinguishable as can be seen in Fig. 9a. The results suggest that [Ca^{2+}]$_o$ shifts the population of conformational ensembles of CaSR to a semi-

active ensemble that can subsequently be shifted to an ensemble of more active conformations upon interaction of the receptor with L-Phe. These results are consistent with the experiments described above and suggest that the unbound CaSR does not respond to L-Phe alone, because L-Phe cannot effectively shift the inactive conformations to an active ensemble of conformations. The above results do not rule out the role of conformational selection, which implies the existence of all relevant active and inactive conformations of the receptor before binding, in the mechanism of activation of CaSR, but clearly indicate that the ensembles of active and inactive conformations are distinctly different and that [Ca^{2+}]$_o$ alone and/or [Ca^{2+}]$_o$ and L-Phe together are required to shift the population, in agreement with previously well documented experimental results that L-Phe could not activate CaSR at sub-threshold levels of [Ca^{2+}]$_o$ (below about 1.0 mM in CaSR-transfected HEK-293 cells) (58).

Based on all the experimental results and the directions of the eigenvectors from the long-time simulation (Fig. 9b) we propose a model to illustrate the possible mechanism by which Ca^{2+} and L-Phe regulate the function of the CaSR mainly through the molecular connectivity encoded at the hinge region of the ECD of the protein. Our model (Fig. 9c) suggests that a local conformational change upon interaction of the CaSR with L-Phe might affect the overall conformation of the receptor, thereby influencing the cooperativity between multiple Ca^{2+}-binding sites and enhancing the receptor's overall response to Ca^{2+}.

Discussion

Several major barriers have hampered our understanding of how CaSR integrates its activation by two different classes of nutrients, divalent cations and amino acids, to regulate the functional cooperativity of the receptor and of the alterations of this cooperativity caused by disease mutations. These include "invisible" binding pockets for these two key physiological agonists of the CaSR, namely Ca^{2+} and amino acids, challenges in obtaining structural information associated with membrane proteins, and the lack

of direct binding methods in determining the mechanism underlying cooperative activation of the CaSR by Ca^{2+} and amino acids (13,19,59). To overcome these limitations, we have developed several computer algorithms and a grafting approach for identifying and predicting Ca^{2+}-binding sites in proteins, and we have successfully verified the intrinsic Ca^{2+}-binding capabilities of predicted Ca^{2+}-binding sites in the CaSR and mGluR1α (25-27,60).

Our studies, shown in Figs. 1, 3 and 6, suggest that mutations in Ca^{2+}-binding Site 1, such as E2971 and Y218Q, not only disrupt the CaSR's Ca^{2+}-sensing capacity but also have an impact on the positive homotropic cooperative interactions of Ca^{2+} with the other Ca^{2+}-binding sites. The biphasic behavior of these mutants with a large disruption of cooperativity is very similar to our previously reported metal-binding concentration response curves of subdomain 1 and its variants with increases in [Ca^{2+}]$_o$ (26). Subdomain 1 of CaSR contains a protein sequence encompassing Ca^{2+}-binding Sites 1, 2 and 3, but not Ca^{2+}-binding Sites 4 and 5. It also exhibits both a strong and a weak metal-binding component. This strong metal-binding process can be removed by further mutating Site 1 (E297I). In contrast, mutations at Sites 2 and 3 in subdomain 1 have less impact on the first binding process (26). These experimental results are consistent with molecular dynamics simulation studies carried out here showing that residues located at Site 1 have strong correlated motions with other residues involved in Sites 2, 3, 4 and 5 (Table 1). The results suggest that the dynamics of Site 1 are intricately coupled to those of the other binding sites; therefore, any changes in the dynamics of Site 1 could affect those of the other sites. The observation of this molecular connectivity and its relationship to positive cooperativity from the molecular dynamics simulations provides a description at the atomic level of the crosstalk between the different sites of the CaSR suggested by the experimental results in live cells.

Here, we have also identified and characterized an L-Phe-binding pocket formed by residues L51, S170, T145, Y218 and S272 that is adjacent to and partially overlaps the key Ca^{2+}-binding Site 1 at the hinge region of the Venus Fly Trap (VFT) of the CaSR. This Ca^{2+}-binding Site is also conserved in other family C GPCRs, including the mGluR1 VFT (Fig. 2) (27,31,56). Y218 is involved in sensing both Ca^{2+} and L-Phe. The aromatic ring from residue Y218 could form delocalized pi bonds with the side chain of L-Phe and the hydrophobic interaction between L51 and L-Phe would further stabilize this interaction. Mutating S170 might interfere with H-bonding of the ligated amino acid to the α-amino group of S170 based on the structure of mGluR1α (53). S170T has been reported by different groups to interfere with the CaSR's L-Phe-sensing ability (51,53). Consideration of the crystal structure of the glutamate-bound form of mGluR1 (31), together with our docking analysis, implies that residues T145 and S272 may not directly participate in the interaction with L-Phe but could possibly interact with L-Phe by ligation of water molecules, which is a relatively weaker type of interaction.

We have observed essentially equivalent expression of WT CaSR as well as its variants on the cell surface (Fig. 5). These data suggest that the difference in the Ca^{2+}-sensing capacities among the WT and mutant receptors are due to perturbation of the cell surface receptors' functions, rather than, for example, impaired trafficking of the receptor proteins to the cell surface. L-Phe rescued the calcium responses of the tested mutants located in all five predicted Ca^{2+}-binding sites, and it had more dramatic rescuing effects on mutants E297I and D215I compared with the other mutants (Fig. 8d). Thus, the importance of the hinge region, where L-Phe likely interacts with the CaSR ECD, is once again highlighted.

The PCA results suggest that the need for Ca^{2+} in initially activating CaSR, as suggested by these experiments, is related to shifting the ensemble of conformations of CaSR from an inactive state to an active state. The activity of the Ca^{2+}-loaded form of CaSR is then further enhanced by the binding of L-Phe, which produces an additional change in the ensembles of conformations of CaSR. Therefore, the global modulation of receptor activity by Ca^{2+} and L-Phe

might be explained by a combination of an induced fit and population shift models (61), that is the receptor's overall structure could vary in the equilibrium distributions of conformations that can interchange dynamically in the absence of Ca^{2+} and L-Phe . Our experimental results suggest that binding of Ca^{2+} at its various sites is associated with motions of these sites that are highly correlated with one another. Consequently, the shift in the ensemble of conformations of CaSR induced by the initial binding of Ca^{2+} at Site 1 will alter the equilibrium population of the unbound conformations of other Ca^{2+}-binding sites due to their crosstalk with Site 1. The binding of Ca^{2+} to Site 1 and the subsequent interaction of CaSR with L-Phe can further shift the conformations of the ECD from one part of the free energy landscape to another. In this way Ca^{2+}-binding to other sites is more readily favorable. Our findings here also enhance our understanding of the role of Ca^{2+} in modulating key Ca^{2+}-binding proteins, such as calmodulin, to mediate signal transduction via correlated motions among their multiple Ca^{2+}-binding sites, thereby generating cooperative responses with critical biological consequences (62,63).

The CaSR's co-activation by these two classes of ligands may be particularly important in the gastrointestinal tract, where high concentrations of amino acids resulting from protein digestion would promote activation of the CaSR and its stimulation of digestive processes even when there are relatively low levels of [Ca^{2+}]$_o$. Moreover, as reported in clinical studies, there are 33 disease-related variants near Ca^{2+}-binding Site 1 associated with receptor activation or inactivation and, in some cases, with reduced cooperativity (15). Our work suggests that it is likely that such mutations disrupt the molecular connectivity encoded in the receptor and provide a better understanding of the molecular basis of some of the CaSR-related clinical disorders. Although the circulating levels of Ca^{2+} and L-Phe *in vivo* are lower than in the *in vitro* experiments, the discrepancy noted here (2-3-fold for the WT receptor for Ca^{2+}) is substantially less than variety of more classical hormone-receptor systems. For the cloned parathyroid hormone (PTH) receptor,

for example, the K$_d$'s for activation of adenylate cyclase and stimulation of PLC, are 1 nM and 20-50 nM, respectively, while the normal circulating levels of PTH are ~1-7 pM, i.e., resulting in a >100-fold to even a >1000-fold discrepancy between *in vivo* and *in vitro* results (64). Our finding of the capacity of L-Phe to rescue disease-linked mutations suggests the possibility of enhancing the activities of such mutant receptors using calcimimetics of various types as pharmacotherapy. Thus our results provide insights into key factors regulating the receptor's overall activity, which can lay the foundation for a new generation of therapeutics and drugs.

In addition to the Ca^{2+}-sensing receptor, [Ca^{2+}]$_o$ regulates 14 of the other members of the family C G protein-coupled receptors (GPCRs), including the metabotropic glutamate receptors (mGluR), γ-aminobutyric acid GABA$_B$ receptors and receptors for pheromones, amino acids and sweet substances (1,5,10,16,54-56,65). The observed molecular connectivity centered at predicted calcium-binding Site 1 of the CaSR, which is adjacent to an amino acid-binding pocket at the hinge region of the receptor, may be shared by other members of the family C GPCRs (66,67) . Besides the strong conservation of the predicted calcium-binding site 1 and the adjacent amino acid-binding pocket, several lines of evidence support this suggestion (Fig. 2) (25,26,56,68). We have predicted a Ca^{2+}-binding site partially sharing a Glu-binding site in the ECD of mGluR1 α , and both of them co-activate the receptor (27). A Ca^{2+}-binding pocket was proposed to be present in the ligand-binding site of the GABA$_B$ receptor (55). Many animals and humans can detect the taste of calcium via a calcium taste receptor that is modulated by an allosteric mechanism (69).

In summary, our present study provides a mechanistic view of the interplay among extracellular Ca^{2+}, amino acids and the CaSR via molecular connectivity that modulates the positive homotropic and heterotropic cooperativity of CaSR-mediated intracellular Ca^{2+} signaling. The positive cooperative co-activation of the CaSR by Ca^{2+} and L-Phe and the importance of the positive homotropic and heterotropic cooperativity, respectively, exhibited by the two agonists may be

further extended to other members of the family C GPCRs to facilitate understanding molecular basis for related human disorders and the development of new therapeutic strategies.

References:
1. Brown, E. M., Gamba, G., Riccardi, D., Lombardi, M., Butters, R., Kifor, O., Sun, A., Hediger, M. A., Lytton, J., and Hebert, S. C. (1993) Cloning and characterization of an extracellular Ca^{2+}-sensing receptor from bovine parathyroid. *Nature* **366**, 575-580
2. Chang, W., and Shoback, D. (2004) Extracellular Ca^{2+}-sensing receptors--an overview. *Cell Calcium* **35**, 183-196
3. Breitwieser, G. E. (2006) Calcium sensing receptors and calcium oscillations: calcium as a first messenger. *Curr. Top Dev. Biol.* **73**, 85-114
4. Huang, C., and Miller, R. T. (2007) The calcium-sensing receptor and its interacting proteins. *J. Cell. Mol. Med.* **11**, 923-934
5. Wellendorph, P., and Brauner-Osborne, H. (2009) Molecular basis for amino acid sensing by family C G-protein-coupled receptors. *Br. J. Pharmacol.* **156**, 869-884
6. Cheng, S. X., Geibel, J. P., and Hebert, S. C. (2004) Extracellular polyamines regulate fluid secretion in rat colonic crypts via the extracellular calcium-sensing receptor. *Gastroenterology* **126**, 148-158
7. Tu, C. L., Oda, Y., Komuves, L., and Bikle, D. D. (2004) The role of the calcium-sensing receptor in epidermal differentiation. *Cell Calcium* **35**, 265-273
8. Mathias, R. S., Mathews, C. H., Machule, C., Gao, D., Li, W., and Denbesten, P. K. (2001) Identification of the calcium-sensing receptor in the developing tooth organ. *J. Bone Miner. Res.* **16**, 2238-2244
9. Buchan, A. M., Squires, P. E., Ring, M., and Meloche, R. M. (2001) Mechanism of action of the calcium-sensing receptor in human antral gastrin cells. *Gastroenterology* **120**, 1128-1139
10. Hofer, A. M., and Brown, E. M. (2003) Extracellular calcium sensing and signalling. *Nat. Rev. Mol. Cell Biol.* **4**, 530-538
11. Brown, E. M., and MacLeod, R. J. (2001) Extracellular calcium sensing and extracellular calcium signaling. *Physiol. Rev.* **81**, 239-297
12. Dolmetsch, R. E., Xu, K., and Lewis, R. S. (1998) Calcium oscillations increase the efficiency and specificity of gene expression. *Nature* **392**, 933-936
13. Miedlich, S., Gama, L., and Breitwieser, G. E. (2002) Calcium sensing receptor activation by a calcimimetic suggests a link between cooperativity and intracellular calcium oscillations. *J. Biol. Chem.* **277**, 49691-49699
14. Young, S. H., and Rozengurt, E. (2002) Amino acids and Ca^{2+} stimulate different patterns of Ca^{2+} oscillations through the Ca^{2+}-sensing receptor. *Am. J. Physiol. Cell Physiol.* **282**, C1414-1422

15. Hannan, F. M., Nesbit, M. A., Zhang, C., Cranston, T., Curley, A. J., Harding, B., Fratter, C., Rust, N., Christie, P. T., Turner, J. J., Lemos, M. C., Bowl, M. R., Bouillon, R., Brain, C., Bridges, N., Burren, C., Connell, J. M., Jung, H., Marks, E., McCredie, D., Mughal, Z., Rodda, C., Tollefsen, S., Brown, E. M., Yang, J. J., and Thakker, R. V. (2012) Identification of 70 calcium-sensing receptor mutations in hyper- and hypo-calcaemic patients: evidence for clustering of extracellular domain mutations at calcium-binding sites. *Hum. Mol. Genet.* **21**, 2768-2778

16. Hu, J., and Spiegel, A. M. (2003) Naturally occurring mutations of the extracellular Ca^{2+}-sensing receptor: implications for its structure and function. *Trends Endocrinol. Metab.* **14**, 282-288

17. Hendy, G. N., Guarnieri, V., and Canaff, L. (2009) Calcium-sensing receptor and associated diseases. *Prog. Mol. Biol. Transl. Sci.* **89**, 31-95

18. Francesconi, A., and Duvoisin, R. M. (2004) Divalent cations modulate the activity of metabotropic glutamate receptors. *J. Neurosci. Res.* **75**, 472-479

19. Conigrave, A. D., Quinn, S. J., and Brown, E. M. (2000) L-amino acid sensing by the extracellular Ca^{2+}-sensing receptor. *Proc. Natl. Acad. Sci. U.S.A.* **97**, 4814-4819

20. Wang, M., Yao, Y., Kuang, D., and Hampson, D. R. (2006) Activation of family C G-protein-coupled receptors by the tripeptide glutathione. *J. Biol. Chem.* **281**, 8864-8870

21. Conigrave, A. D., Mun, H. C., and Lok, H. C. (2007) Aromatic L-amino acids activate the calcium-sensing receptor. *J. Nutr.* **137**, 1524S-1527S; discussion 1548S

22. Conigrave, A. D., and Brown, E. M. (2006) Taste receptors in the gastrointestinal tract. II. L-amino acid sensing by calcium-sensing receptors: implications for GI physiology. *Am. J. Physiol. Gastrointest Liver Physiol.* **291**, G753-761

23. Liou, A. P., Sei, Y., Zhao, X., Feng, J., Lu, X., Thomas, C., Pechhold, S., Raybould, H. E., and Wank, S. A. (2011) The extracellular calcium-sensing receptor is required for cholecystokinin secretion in response to L-phenylalanine in acutely isolated intestinal I cells. *Am. J. Physiol. Gastrointest Liver Physiol.* **300**, G538-546

24. Broadhead, G. K., Mun, H. C., Avlani, V. A., Jourdon, O., Church, W. B., Christopoulos, A., Delbridge, L., and Conigrave, A. D. (2011) Allosteric modulation of the calcium-sensing receptor by gamma-glutamyl peptides: inhibition of PTH secretion, suppression of intracellular cAMP levels, and a common mechanism of action with L-amino acids. *J. Biol. Chem.* **286**, 8786-8797

25. Huang, Y., Zhou, Y., Yang, W., Butters, R., Lee, H. W., Li, S., Castiblanco, A., Brown, E. M., and Yang, J. J. (2007) Identification and dissection of Ca^{2+}-binding sites in the extracellular domain of Ca^{2+}-sensing receptor. *J. Biol. Chem.* **282**, 19000-19010

26. Huang, Y., Zhou, Y., Castiblanco, A., Yang, W., Brown, E. M., and Yang, J. J. (2009) Multiple Ca^{2+}-binding sites in the extracellular domain of the Ca^{2+}-sensing receptor corresponding to cooperative Ca^{2+} response. *Biochemistry* **48**, 388-398

27. Jiang, Y., Huang, Y., Wong, H. C., Zhou, Y., Wang, X., Yang, J., Hall, R. A., Brown, E. M., and Yang, J. J. (2010) Elucidation of a novel extracellular calcium-binding site on metabotropic glutamate receptor 1α (mGluR1α) that controls receptor activation. *J. Biol. Chem.* **285**, 33463-33474

28. Trott, O., and Olson, A. J. (2010) AutoDock Vina: improving the speed and accuracy of docking with a new scoring function, efficient optimization, and multithreading. *J. Comput. Chem.* **31**, 455-461

29. Sobolev, V., Sorokine, A., Prilusky, J., Abola, E. E., and Edelman, M. (1999) Automated analysis of interatomic contacts in proteins. *Bioinformatics* **15**, 327-332

30. Huang, Y., Zhou, Y., Wong, H. C., Castiblanco, A., Chen, Y., Brown, E. M., and Yang, J. J. (2010) Calmodulin regulates Ca^{2+}-sensing receptor-mediated Ca^{2+} signaling and its cell surface expression. *J. Biol. Chem.* **285**, 35919-35931

31. Kunishima, N., Shimada, Y., Tsuji, Y., Sato, T., Yamamoto, M., Kumasaka, T., Nakanishi, S., Jingami, H., and Morikawa, K. (2000) Structural basis of glutamate recognition by a dimeric metabotropic glutamate receptor. *Nature* **407**, 971-977

32. Case, D. A., Darden, T. A., Cheatham, I., T. E. ; , Simmerling, C. L., Wang, J., Duke, R. E., Luo, R., Crowley, M., Walker, R. C., Zhang, W., Merz, K. M., Wang, B., Hayik, S., Roitberg, A., Seabra, G., Kolossváry, I., Wong, K. F., Paesani, F., Vanicek, J., Wu, X., Brozell, S. R., Steinbrecher, T., Gohlke, H., Yang, L., Tan, C., Mongan, J., Hornak, V., Cui, G., Mathews, D. H., Seetin, M. G., Sagui, C., Babin, V., and Kollman, P. A. (2008) AMBER 10. University of California, San Francisco.

33. Jorgensen, W. L., Chandrasekhar, J., Madura, J. D., Impey, R. W., and Klein, M. L. (1983) Comparison of simple potential functions for simulating liquid water. *J. Chem. Phys* **79**, 926-935

34. Cornell, W. D., Cieplak, P., Christopher, I. B., Gould, I. R., Merz, J. K. M., Ferguson, D. M., Spellmeyer, D. C., Fox, T., Caldwell, J. W., and Kollman, P. A. (1995) A Second Generation Force Field for the Simulation of Proteins, Nucleic Acids, and Organic Molecules. *J. Am. Chem. Soc.* **117**, 5179-5197

35. Urmi, D., and Hamelberg, D. (2009) Reoptimization of the AMBER Force Field Parameters for Peptide Bond (Omega) Torsions Using Accelerated Molecular Dynamics. *J. Phys. Chem.* **113**, 16590-16595

36. Darden, T., York, D., and Pedersen, L. (1993) Particle mesh Ewald: An N·log(N) method for Ewald sums in large systems. *J. Chem. Phys* **98**, 10089-10092

37. Ryckaert, J. P., Ciccotti, G., and Berendsen, H. J. C. (1977) Numerical integration of the cartesian equations of motion of a system with constraints: molecular dynamics of n-alkanes. *J. Comput. Phys.* **23**, 327-341

38. Doshi Urmi., H. D. (2012) Improved Statistical Sampling and Accuracy with Accelerated Molecular Dynamics on Rotatable Torsions. *J. Chem. Theory Comput.* **8**, 4004-4012

39. Hamelberg, D., de Oliveira, C. A., and McCammon, J. A. (2007) Sampling of slow diffusive conformational transitions with accelerated molecular dynamics. *J. Chem. Phys.* **127**, 155102

40. Mongan, J. (2004) Interactive essential dynamics. *J. Comput. Aided Mol. Des.* **18**, 433-436

41. Levy, R. M., Srinivasan, A. R., Olson, W. K., and McCammon, J. A. (1984) Quasi-harmonic method for studying very low frequency modes in proteins. *Biopolymers* **23**, 1099-1112

42. Jolliffe, I.T. (2002) Principal Component Analysis, *Springer*, New York

43. Bai, M. (2004) Structure-function relationship of the extracellular calcium-sensing receptor. *Cell Calcium* **35**, 197-207

44. Gama, L., Wilt, S. G., and Breitwieser, G. E. (2001) Heterodimerization of calcium sensing receptors with metabotropic glutamate receptors in neurons. *J. Biol. Chem.* **276**, 39053-39059

45. Wang, X., Kirberger, M., Qiu, F., Chen, G., and Yang, J. J. (2009) Towards predicting Ca^{2+}-binding sites with different coordination numbers in proteins with atomic resolution. *Proteins* **75**, 787-798

46. Thakker, R. V. (2004) Diseases associated with the extracellular calcium-sensing receptor. *Cell Calcium* **35**, 275-282

47. Monod, J., Wyman, J., and Changeux, J. P. (1965) On the Nature of Allosteric Transitions: A Plausible Model. *J. Mol. Biol.* **12**, 88-118

48. Koshland, D. E., Jr., Nemethy, G., and Filmer, D. (1966) Comparison of experimental binding data and theoretical models in proteins containing subunits. *Biochemistry* **5**, 365-385

49. Ackers, G. K. (1998) Deciphering the molecular code of hemoglobin allostery. *Adv. Protein Chem.* **51**, 185-253

50. Adcock, S. A., and McCammon, J. A. (2006) Molecular dynamics: survey of methods for simulating the activity of proteins. *Chem. Rev.* **106**, 1589-1615

51. Zhang, Z., Qiu, W., Quinn, S. J., Conigrave, A. D., Brown, E. M., and Bai, M. (2002) Three adjacent serines in the extracellular domains of the CaR are required for L-amino acid-mediated potentiation of receptor function. *J. Biol. Chem.* **277**, 33727-33735

52. Mun, H. C., Franks, A. H., Culverston, E., Krapcho, K., Nemeth, E. F., and Conigrave, A. D. (2004) The Venus Fly Trap domain of the extracellular Ca^{2+}-sensing receptor is required for L-amino acid sensing. *J. Biol. Chem.* **279**, 51739-51744

53. Mun, H. C., Culverston, E. L., Franks, A. H., Collyer, C. A., Clifton-Bligh, R. J., and Conigrave, A. D. (2005) A double mutation in the extracellular Ca^{2+}-sensing receptor's venus flytrap domain that selectively disables L-amino acid sensing. *J. Biol. Chem.* **280**, 29067-29072

54. Wise, A., Green, A., Main, M. J., Wilson, R., Fraser, N., and Marshall, F. H. (1999) Calcium sensing properties of the GABA(B) receptor. *Neuropharmacology* **38**, 1647-1656

55. Galvez, T., Urwyler, S., Prezeau, L., Mosbacher, J., Joly, C., Malitschek, B., Heid, J., Brabet, I., Froestl, W., Bettler, B., Kaupmann, K., and Pin, J. P. (2000) Ca^{2+} requirement for high-affinity gamma-aminobutyric acid (GABA) binding at GABA(B) receptors: involvement of serine 269 of the GABA(B)R1 subunit. *Mol. Pharmacol.* **57**, 419-426

56. Silve, C., Petrel, C., Leroy, C., Bruel, H., Mallet, E., Rognan, D., and Ruat, M. (2005) Delineating a Ca^{2+} binding pocket within the venus flytrap module of the human calcium-sensing receptor. *J. Biol. Chem.* **280**, 37917-37923

57. Christopoulos, A., and Kenakin, T. (2002) G protein-coupled receptor allosterism and complexing. *Pharmacol. Rev.* **54**, 323-374

58. Conigrave, A. D., Franks, A. H., Brown, E. M., and Quinn, S. J. (2002) L-amino acid sensing by the calcium-sensing receptor: a general mechanism for coupling protein and calcium metabolism? *Eur. J. Clin. Nutr.* **56**, 1072-1080

59. Breitwieser, G. E. (2012) Minireview: the intimate link between calcium sensing receptor trafficking and signaling: implications for disorders of calcium homeostasis. *Mol. Endocrinol.* **26**, 1482-1495

60. Bugaj, V., Alexeenko, V., Zubov, A., Glushankova, L., Nikolaev, A., Wang, Z., Kaznacheyeva, E., Bezprozvanny, I., and Mozhayeva, G. N. (2005) Functional properties of endogenous receptor- and store-operated calcium influx channels in HEK293 cells. *J. Biol. Chem.* **280**, 16790-16797

61. Okazaki, K., and Takada, S. (2008) Dynamic energy landscape view of coupled binding and protein conformational change: induced-fit versus population-shift mechanisms. *Proc. Natl. Acad. Sci. U.S.A.* **105**, 11182-11187

62. Gsponer, J., Christodoulou, J., Cavalli, A., Bui, J. M., Richter, B., Dobson, C. M., and Vendruscolo, M. (2008) A coupled equilibrium shift mechanism in calmodulin-mediated signal transduction. *Structure* **16**, 736-746

63. Anthis, N. J., Doucleff, M., and Clore, G. M. (2011) Transient, sparsely populated compact states of apo and calcium-loaded calmodulin probed by paramagnetic relaxation enhancement: interplay of conformational selection and induced fit. *J. Am. Chem. Soc.* **133**, 18966-18974

64. Bringhurst, F. R., Juppner, H., Guo, J., Urena, P., Potts, J. T., Jr., Kronenberg, H. M., Abou-Samra, A. B., and Segre, G. V. (1993) Cloned, stably expressed parathyroid hormone (PTH)/PTH-related peptide receptors activate multiple messenger signals and biological responses in LLC-PK1 kidney cells. *Endocrinology* **132**, 2090-2098

65. Hinson, T. K., Damodaran, T. V., Chen, J., Zhang, X., Qumsiyeh, M. B., Seldin, M. F., and Quarles, L. D. (1997) Identification of putative transmembrane receptor sequences homologous to the calcium-sensing G-protein-coupled receptor. *Genomics* **45**, 279-289

66.   Brauner-Osborne, H., Jensen, A. A., Sheppard, P. O., O'Hara, P., and Krogsgaard-Larsen, P. (1999) The agonist-binding domain of the calcium-sensing receptor is located at the amino-terminal domain. *J. Biol. Chem.* **274**, 18382-18386

67.   Hammerland, L. G., Krapcho, K. J., Garrett, J. E., Alasti, N., Hung, B. C., Simin, R. T., Levinthal, C., Nemeth, E. F., and Fuller, F. H. (1999) Domains determining ligand specificity for Ca²⁺ receptors. *Mol. Pharmacol.* **55**, 642-648

68.   Brauner-Osborne, H., Wellendorph, P., and Jensen, A. A. (2007) Structure, pharmacology and therapeutic prospects of family C G-protein coupled receptors. *Curr. Drug Targets* **8**, 169-184

69.   Tordoff, M. G., Alarcon, L. K., Valmeki, S., and Jiang, P. (2012) T1R3: a human calcium taste receptor. *Sci. Rep.* **2**, 496

70.   Ho, C., Conner, D. A., Pollak, M. R., Ladd, D. J., Kifor, O., Warren, H. B., Brown, E. M., Seidman, J. G., and Seidman, C. E. (1995) A mouse model of human familial hypocalciuric hypercalcemia and neonatal severe hyperparathyroidism. *Nat. Genet.* **11**, 389-394

Footnote

C.Z., Y.H. and J.J.Y. designed the experiments. C.Z. and Y.H. performed the intracellular calcium measurement experiments. Y.H., N.M., D.H.,Y.J., and C.Z characterized the predicted calcium- and L-Phe-binding sites. Y.H., L.W., and C.Z. constructed mutants. N.M. and D.H. carried out computational simulation, C.Z., Y.H., N.M.,Y.J., D.H, E.M.B., and J.J.Y. analyzed data. C.Z., D.H., E.M.B., and J.J.Y. wrote the paper. All authors discussed the results and commented on the manuscript.

Competing financial interests

The author(s) declare no competing financial interests.

Figure legends

Fig. 1. Delineating the molecular connectivity associated with functional positive homotropic and positive heterotropic cooperativity within the CaSR's ECD by molecular modeling of L-Phe- and Ca²⁺-binding sites. The model structure of the ECD of CaSR was based on the mGluR1 crystal structure (PDB entry: 1ISR) and was generated using MODELER 9v4 and Pymol. Upper-right panel: Five predicted Ca²⁺-binding sites are located in the ECD and are highlighted with frames. Residues involved in Ca²⁺-binding are shown in violet. Correlated motions among Ca²⁺-binding Site 1 and the other Ca²⁺-binding sites are shown by lines of various colors. **Upper panel:** A zoomed in view of Site 1; residues involved in the predicted L-Phe-binding site are highlighted in pink. Red: Ca²⁺; Yellow: L-Phe. **Lower panel:** The correlation map of the modeled CaSR ECD structure. The correlation map is depicted based on molecular dynamics (MD) simulations. The strongest negative correlation is given the value -1 while the strongest positive correlation is defined as +1. The circles on the correlation map reflect the movements between different binding sites (corresponding to the correlated motions in the upper-right panel) during the MD simulation.

Fig. 2. Sequence alignment and binding energy calculations based on the MD simulation of modeled CaSR ECD. (a) Sequence alignment of the orthosteric binding site for Glu in mGluR1 with CaSR and

ten other GPCRs of family C. Residues involved in predicted CaSR Ca^{2+}-binding Site 1 are labeled at the top and corresponding residues in other group members are highlighted in yellow. **(b)** The binding energies were calculated from molecular dynamics simulations and docking studies. Red line: CaSR-ECD docking with glutathione (GLUT); Black line: CaSR-ECD docking with phenylalanine (PHE); Blue line: CaSR-ECD docking with aspartic acid (ASP). **(c)**The cross correlation matrices show the movements of residues during MD simulation. Positive values (in red) show residues moving in the same direction while negative values (in blue) indicate residues moving away from one another.

Fig. 3. Intracellular Ca^{2+} responses of CaSR mutants involving various Ca^{2+}-binding sites following simulation with increases in [Ca^{2+}]$_o$. (a). Frequency distribution of the [Ca^{2+}]$_i$ oscillation starting points in HEK-293 cells transfected with WT, E297I or D215I , respectively. The [Ca^{2+}]$_o$ was recorded at the point when single cells started to oscillate. Around 30~60 cells were analyzed and further plotted as a bar chart. **(b).** Population assays of WT and Ca^{2+}-binding site-related mutations. HEK293 cells transfected with CaSR or its mutants were loaded with Fura-2 AM. The intracellular Ca^{2+} level was assessed by monitoring emission at 510 nm with excitation alternately at 340 or 380 nm as described previously (30). The [Ca^{2+}]$_i$ changes in the transfected cells were monitored using fluorimetry during stepwise increases in [Ca^{2+}]$_o$. The [Ca^{2+}]$_i$ responses at various [Ca^{2+}]$_o$ were plotted and further fitted using the Hill equation.

Fig. 4 Individual cellular responses of mutants in calcium-binding sites to the indicated increments of [Ca^{2+}]$_o$ in the presence or absence of L-Phe. **(a)** Representative intracellular calcium response from a single cell. Fura-2-loaded HEK293 cells expressing CaSR with mutations in calcium-binding site 3, 4 or 5 were prepared for single cell experiments. Each experiment with or without 5 mM L-Phe began in the same non-calcium-containing Ringer's buffer followed by stepwise increases in [Ca^{2+}]$_o$ as indicated above the oscillation pattern using a perfusion system until [Ca^{2+}]$_i$ reached a plateau (up to 30 mM [Ca^{2+}]$_o$). At least 30 cells were analyzed for each mutant. **(b)** Frequency distribution of the [Ca^{2+}]$_o$ at which CaSR-transfected single HEK293 cells started to oscillate. The cell number % is defined as the number of cells starting to oscillate at a given [Ca^{2+}]$_o$/total cell number showing oscillation pattern x 100. Empty bar: in the absence of L-Phe; Black bar: in the presence of 5 mM L-Phe. **(c)** The frequency distribution of the oscillation frequency from single cells was investigated as described before. For experiments without L-Phe, the peaks per minute were recorded at the level of [Ca^{2+}]$_o$ at which the majority of the cells (>50%) started to oscillate; for experiments with 5.0 mM L-Phe, the frequency was analyzed at the same [Ca^{2+}]$_o$ that was used in the absence of L-Phe. Specifically, the frequency of E224I was studied at 4 mM [Ca^{2+}]$_o$; E353I was analyzed at 5.0 mM [Ca^{2+}]$_o$; D398A/E399I was investigated at 10.0 mM [Ca^{2+}]$_o$ and . Empty bar: in the absence of L-Phe; black bar: in the presence of 5 mM L-Phe.

Fig. 5 Expression of WT CaSR and its mutants in HEK293 cells. (a) Western blot analyses of CaSR and its mutants in transiently transfected HEK293 cells. 40 μg of total protein from cellular lysates were subjected to 8.5% SDS-PAGE. Three characteristic bands are shown in the upper panel, including the top band representing the dimeric receptor, the middle band showing mature glycosylated CaSR monomer (150 kDa), and the lowest band indicating immature glycosylated CaSR monomer (130 kDa). (b) Quantification of the expression of WT CaSR and its mutants in HEK293 cells. All the bands including the one indicating dimeric receptor, mature glycosylated monomer and the one showing immature CaSR monomer were taken into consideration. The internal control GAPDH was used to standardize CaSR expression and the mutants were further normalized to the WT CaSR expression. **(c)** Immunofluorescence analyses of surface expressed WT CaSR and its mutants in HEK293 cells. Immunostaining was done with anti-CaSR monoclonal antibody ADD (70), and detection was carried out with Alex Fluor 488-conjugated, goat anti-mouse secondary antibody. Red, PI staining of cell nuclei; Green, CaSR. Equivalent expression of WT CaSR as well as its variants on the cell surface suggests that the difference in the Ca^{2+}-

16

sensing capabilities among the WT and mutant receptors are due to perturbation of the cell surface receptors' functions, rather than, for example, impaired trafficking of the receptor proteins to the cell surface.

Fig. 6. Functional studies of receptors with mutations in L-Phe-binding site in HEK293 cells. (a). Representative oscillation pattern from a single cell. Each experiment with or without 5 mM L-Phe began in Ca^{2+}-free Ringer's buffer followed by stepwise increases in [Ca^{2+}]$_o$ until [Ca^{2+}]$_i$ reached a plateau (up to 30 mM [Ca^{2+}]$_o$). **(b).** The pattern of [Ca^{2+}]$_i$ responses in each cell (minimum of 30 cells) was analyzed, and the [Ca^{2+}]$_o$ at which individual cells started to oscillate was recorded and plotted as a bar chart. **(c).** The frequency of the oscillation patterns of the individual cells was investigated. For experiments without L-Phe, the peaks per minute were recorded at the level of [Ca^{2+}]$_o$ at which the majority of the cells (>50%) started oscillating; while for experiments with 5 mM L-Phe, the frequency was analyzed at the same levels of [Ca^{2+}]$_o$ as in the corresponding experiments carried out without L-Phe. **(d).** Population assay for [Ca^{2+}]$_i$ responses of HEK293 cells transiently overexpressing WT CaSR or CaSR mutants L51A or Y218Q using Fura-2 AM during stepwise increases in [Ca^{2+}]$_o$ from 0.5 to 30 mM. The ratio of the intensity of light emitted at 510 nm upon excitation with 340 or 380 nm was normalized to its maximum response. The [Ca^{2+}]$_o$ concentration response curves were fitted using the Hill equation.

Fig. 7 Individual cellular responses of mutants in the L-Phe-sensitive site to the indicated increments of [Ca^{2+}]$_o$ in the presence or absence of L-Phe. HEK-293 cells transfected with wild type CaSR or mutants were loaded with Fura-2 AM for 15 min. Each experiment with or without 5 mM L-Phe began in the same non-calcium-containing Ringer's buffer followed by stepwise increases in [Ca^{2+}]$_o$ until [Ca^{2+}]$_i$ reached a plateau (up to 30 mM) as monitored by changes in the ratio of light emitted at 510 nm following excitation at 340 or 380 nm. At least 30 cells were analyzed for mutants S272A and T145A. Representative cellular responses from a single cell are shown.

Fig. 8. [Ca^{2+}]$_i$ responses of CaSRs with mutations in the Ca^{2+}-binding sites stimulated by increasing [Ca^{2+}]$_o$ in the presence or absence of 5 mM L-Phe. (a). [Ca^{2+}]$_i$ was monitored in mutants E297I and D215I in the absence or presence of L-Phe. [Ca^{2+}]$_o$ was increased stepwise up to 30 mM or until [Ca^{2+}]$_i$ reached a plateau. (b). Frequency distribution of [Ca^{2+}]$_o$ at which CaSR-transfected single HEK293 cells started to oscillate. **(c).** In the single cell experiments, the frequency of the oscillation patterns was investigated in more than 30 cells. For experiments without L-Phe, the peaks per minute were recorded at the level of [Ca^{2+}]$_o$ at which the majority of the cells (>50%) started to oscillate, while for experiments with 5 mM L-Phe, the frequency was analyzed at the corresponding level of [Ca^{2+}]$_o$ that was studied in the absence of L-Phe. Empty bar: in the absence of L-Phe; Black bar: in the presence of 5 mM L-Phe. **(d).** Population assay for measuring [Ca^{2+}]$_i$ responses of HEK293 cells transiently transfected with Ca^{2+}-binding site-related CaSR mutants using Fura-2 AM during stepwise increases in [Ca^{2+}]$_o$ from 0.5 to 30 mM. [Ca^{2+}]$_i$ responses were further fitted using the Hill equation. Inlet: zoomed in view of the binding first phase.

Fig. 9. Principal component analysis (PCA) of CaSR ECD, combined with experimental data, suggest a model for the mechanism underlying activation of the CaSR by extracellular Ca^{2+} and L-Phe. (a). Principal component analysis (PCA) of CaSR ECD. The trajectories of the molecular dynamics simulations were analyzed using principal component analysis (PCA), which separates out the motions of the CaSR ECD into principal modes ranked according to their relative contributions. The first three principal modes were included in the present study to analyze four different states of the protein: Ligand-

free (black), presence of L-Phe-only (Green), presence of Ca^{2+}-only (Red) or presence of both Ca^{2+} and L-Phe (Blue). The superposition of the last snapshots of the aforementioned simulation systems is shown in the right panel. Ca^{2+} is shown as the black sphere; residues involved in Ca^{2+} binding site1 are shown in bond representation; L-Phe is shown as a ball and stick model. **(b).** Representations of the four slowest principal components of the ECD of CaSR using the eigenvectors mapped onto the backbone C atoms of CaSR. The directions of the eigenvectors indicate the bending and twisting motions of the ECD of CaSR. **(c).** Model for the mechanism underlying activation of the CaSR by extracellular Ca^{2+} and L-Phe. Ca^{2+} and L-Phe modulate the activity as well as the cooperativity of CaSR (the color changes of the calcium binding sites from yellow to red indicates an increase in cooperativity). Higher [Ca^{2+}]$_o$, around 3.0 mM, could change the conformation of CaSR into an active form (second stair level) in a positive homotropic cooperative manner (as indicated by the change of the color of the Ca^{2+}-binding sites from yellow to orange) and further trigger [Ca^{2+}]$_i$ oscillations. L-Phe binds to the hinge region between Lobe 1 and Lobe 2, modulating the receptor together with Ca^{2+} in a positive heterotropic cooperative way (as indicated by the change in the color from orange to red). This could produce a conformation of the receptor that is a "super-activated" form (third stair level), associated with a higher frequency of [Ca^{2+}]$_i$ oscillations and a left-shifted EC$_{50}$. CaSR mutants (lower activity stair level), especially those containing mutations close to the hinge region between lobe 1 (LB$_1$) and lobe 2 (LB$_2$) (show in black truncated circle), could cause a disruption of the cooperativity among the various Ca^{2+}-binding sites (lower level, middle stair). [Ca^{2+}]$_o$, at 3.0 mM does not trigger [Ca^{2+}]$_i$ oscillations in the mutant CaSR. The impaired receptor function and the cross talk between Ca^{2+}-binding sites can be rescued, at least in part, by introducing L-Phe into the extracellular buffer (lower level, left stair). Red
Arrow: receptor activity.

Table 1. Analysis of correlated motions of WT CaSR model structure.

The cross-correlation coefficients of each residue to all of the other residues of the modeled CaSR ECD structure after docking with calcium were calculated from the simulation. The strongest positive correlation of a residue with itself is given the value 1; the strongest negative correlation between two residues is given the value -1. A cut off at > 0.7 and < -0.4 is considered as a strong correlation between residues. Strongly correlated residues in predicted calcium-binding sites are listed in the table.

	Residue Pairs
Negative Correlation	S170 (Site 1): D398 (Site 5)
	D190 (Site 1): S244 (Site 2)
	D190 (Site 1): D248 (Site 2)
	E297 (Site 1): D248 (Site 2)
	D190 (Site 1): Q253 (Site 2)
	E297 (Site 1): Q253 (Site 3)
	E218 (Site 1): E350 (Site 4)
	E297 (Site 1): E378 (Site 5)
Positive Correlation	E224 (Site 3): E228 (Site 3)
	E228 (Site 3): E229 (Site 3)
	S244 (Site 2): D248 (Site 2)
	S244 (Site 2): Q253 (Site 2)
	E350 (Site 4): E353 (Site 4)
	E354 (Site 4): E353 (Site 4)
	E378 (Site 5): E379 (Site 5)
	D398 (Site 5): E399 (Site 5)

Table 2 Summary of individual cellular responses to the indicated increments of $[Ca^{2+}]_o$ in HEK293 cells transiently transfected with WT CaSR or mutations in the indicated Ca^{2+}-binding sites.

HEK293 cells were seeded on coverslips one day prior to transient transfection with the WT CaSR or Ca^{2+}-binding-related CaSR mutants. After 48 h, the cells were loaded with fura-2 as described in "Materials and Methods". The level of $[Ca^{2+}]_o$ was recorded at which $[Ca^{2+}]_i$ oscillation started or reached a plateau, which are referred to as the starting point and ending point, respectively. For experiments without L-Phe, the frequency (peaks per minute) was recorded at the level of $[Ca^{2+}]_o$ at which the majority of the cells (>50%) started to oscillate, while for experiments with 5 mM L-Phe, the frequency was analyzed at the corresponding level of $[Ca^{2+}]_o$ that was studied in the absence of L-Phe. Specifically, the frequency was studied at 3.0 mM $[Ca^{2+}]_o$, for WT, 12.5 mM $[Ca^{2+}]_o$ for E297I, 10.0 mM $[Ca^{2+}]_o$ for D215I and D398A/E399I, 4 mM $[Ca^{2+}]_o$ for E224I; and 5.0 mM $[Ca^{2+}]_o$ for E353I.More than 30 cells were analyzed from total 3 independent experiments. Values are means ± S.E. N/A= not available.

Predicted Sites	Residues	Mutants	Starting Point (mM)		Ending Point (mM)		Frequency	
			w/o L-Phe	w L-Phe	w/o L-Phe	w L-Phe	w/o L-Phe	w L-Phe
WT		WT	3.0 ± 0.1	2.0 ± 0.2[b]	6.4 ± 0.3	4.3 ± 0.2	1.5 ± 0.1	2.2 ± 0.2[b]
Site 1	S147, S170,D190, Y218, E297	E297I	17.0 ± 0.4[a]	7.3 ± 0.2[b]	N/A	N/A	1.6 ± 0.1	2.9 ± 0.1[b]
Site 2	D215, L242, S244, D248, Q253	D215I	13.9 ± 0.2[a]	6.7 ± 0.3[b]	N/A	17.7 ± 0.3	1.8 ± 0.1	2.5 ± 0.2[b]
Site 3	E224, E228, E229, E231, E232	E224I	5.0 ± 0.2[a]	3.2 ± 0.1[b]	16.8 ± 0.3	11.0 ± 0.1[b]	1.4 ± 0.2	2.2 ± 0.1[b]
Site 4	E350, E353, E354, N386, S388	E353I	3.4 ± 0.1[a]	2.4 ± 0.1[b]	10.8 ± 0.2	4.9 ± 0.2[b]	1.2 ± 0.2	2.0 ± 0.2[b]
Site 5	E378,E379, T396, D398, E399	D398A /E399I	9.3 ± 0.1[a]	5.5 ± 0.2[b]	N/A	N/A	1.4 ± 0.2	2.2 ± 0.2[b]

[a] indicates significance with respect to wild type CaSR without L-Phe, p <0.05; [b] indicates significance with respect to the corresponding experiment in the same mutant without L-Phe, p <0.05.

Table 3 Summary of EC_{50} values and Hill coefficients predicted using Hill equation for the WT and mutant CaSRs.

HEK293 cells were transiently transfected with the WT CaSR or Ca^{2+}-binding-related CaSR mutants, and after 48 h the cells were loaded with fura-2 as described under "Materials and Methods". The cells on glass coverslips were then transferred into the cuvette for fluorimetry and exposed to various increases in $[Ca^{2+}]_o$ (from 0.5~30 mM) in the absence or presence of 5 mM L-Phe as described above.. The average of $[Ca^{2+}]_i$ at each $[Ca^{2+}]_o$ was plotted against $[Ca^{2+}]_o$ and further fitted using the Hill equation, which gave EC_{50} and Hill numbers. The maximum response for each mutant was subtracted from the baseline and normalized to the maximal cumulative $[Ca^{2+}]_i$ response of the WT receptor. The data were obtained from three experiments for each construct.

Sites	Mutants	Response at 30 mM $[Ca^{2+}]$		$EC_{50}[Ca^{2+}]_o$		Hill Coefficient	
		w/o L-Phe	w L-Phe	w/o L-Phe	w L-Phe	w/o L-Phe	w L-Phe
WT		100.0 ± 2.0	104.6± 2.9	2.9 ± 0.2	1.9 ± 0.2[b]	3.0 ± 0.1	4.0 ± 0.4[b]
Site 1	E297I	78.0 ± 6.9[a]	132.8 ± 1.9[b]	Phase 1: 3.2 ± 0.4 Phase 2: 17.8 ± 0.5	7.4 ± 0.6[b]	Phase 1: 2.8 ± 0.2 Phase 2: 3.5 ± 0.1	4.2 ± 0.3[b]
Site 2	D215I	88.0 ± 2.5[a]	147.5 ± 6.0[b]	14.7 ± 1.9[a]	9.0 ± 0.5[b]	2.0 ± 0.2[a]	2.8 ± 0.3[b]
Site 3	E224I	83.2 ± 5.2[a]	104.2 ± 4.5[b]	5.3 ± 0.4[a]	3.1 ± 0.1[b]	1.9 ± 0.1[a]	4.3 ± 0.2[b]
Site 4	E353I	80.7 ± 1.6[a]	88.9 ± 1.8[b]	4.0 ± 0.1[a]	2.6 ± 0.1[b]	2.3 ± 0.1[a]	3.6 ± 0.1[b]
Site 5	D398A/E399I	80.9 ± 7.0[a]	78.3 ± 6.5	4.7 ± 0.7[a]	3.3 ± 0.1[a]	2.4 ± 0.1[a]	3.6 ± 0.4[b]

[a] indicates significance with respect to wild type CaSR in the absence of L-Phe, $p < 0.05$; [b] indicates significance with respect to the corresponding mutants in the absence of L-Phe, $p < 0.05$.

21

Table 4 Summary of cellular responses of HEK293 cells transiently transfected with WT CaSR or mutants in the predicted L-Phe-binding site.

The average $[Ca^{2+}]_o$ at which cells started $[Ca^{2+}]_i$ oscillations was recorded using the aforementioned methods for WT or each mutant CaSR. For the oscillation frequency in the absence of L-Phe, peaks per minute were measured at the level of $[Ca^{2+}]_o$ at which more than 50% cells started to oscillate; when L-Phe was added, frequencies were recorded at the same $[Ca^{2+}]_o$ as their counterparts without L-Phe. Specifically, the frequencies of WT and L51A was measured at 3.0 mM $[Ca^{2+}]_o$; whileS272A, T145A, and S170T were measured at 2.5 mM $[Ca^{2+}]_o$; and Y218Q was analyzed at 15.0 mM $[Ca^{2+}]_o$. Values are means ± S.E. EC_{50} and Hill numbers obtained from the cell population assay by fitting plots using the Hill equation.

Mutant	Starting Point (mM)		Frequency (Peaks/Min)		EC_{50} (mM)		Hill Number	
	w/o L-Phe	w L-Phe	w/o L-Phe	w L-Phe	w/o L-Phe	w L-Phe	w/o L-Phe	w L-Phe
WT	3.0 ± 0.1	2.0 ± 0.2[b]	1.5 ± 0.1	2.2 ± 0.2[b]	2.9 ± 0.1	1.8 ± 0.2[b]	3.2 ± 0.3	4.1 ± 0.1[b]
L51A	2.9 ± 0.1	2.8 ± 0.1	1.7 ± 0.1	1.8 ± 0.1	3.5 ± 0.2	3.2 ± 0.1	2.7 ± 0.1	2.8 ± 0.2
T145A	2.8 ± 0.1	2.4 ± 0.2[b]	1.7 ± 0.3	1.8 ± 0.2	3.0 ± 0.1	3.0 ± 0.1	3.3 ± 0.3	3.7 ± 0.4
S170T	2.1 ± 0.2[a]	2.0 ± 0.1	1.5 ± 0.1	1.4 ± 0.2	2.7 ± 0.2	2.9 ± 0.1	2.4 ± 0.3	2.2 ± 0.1
Y218Q	17.7 ± 1.0[a]	16.7 ± 2.2	1.5 ± 0.1	1.6 ± 0.1	Phase 1: 3.7 ± 0.4 Phase 2: 27.1 ± 0.8	Phase 1: 3.6 ± 0.2 Phase 2: 24.6 ± 0.5	Phase 1: 3.8 ± 1.0 Phase 2: 3.4 ± 0.5	Phase 1: 3.9 ± 0.4 Phase 2: 2.8 ± 0.8
S272A	2.7 ± 0.2	2.1 ± 0.1[b]	2.3 ± 0.1	2.4 ± 0.1	2.4 ± 0.1	2.2 ± 0.1	1.9 ± 0.1	3.0 ± 0.1

[a] significant difference between mutant receptor and WT CaSR without L-Phe, p<0.05; [b] significant difference between cases without L-Phe and with 5 mM L-Phe, p<0.05.

Table 5. Summary of cellular responses from HEK293 cells transiently transfected with WT CaSR or mutants in the predicted L-Phe-sensing site.

The intracellular calcium responses of HEK293 cells transiently overexpressing WT CaSR or various mutants potentially involved in the interaction with L-Phe were measured using Fura-2AM during stepwise increases in $[Ca^{2+}]_o$. The pattern of $[Ca^{2+}]_i$ responses in each cell (minimum of 30 cells) was analyzed, and the $[Ca^{2+}]_o$ at which individual cells started to oscillate was recorded. For experiments without L-Phe, the peaks per minute were recorded at the level of $[Ca^{2+}]_o$ at which the majority of the cells (>50%) started oscillating; while for experiments with 5 mM L-Phe, the frequency was analyzed at the same levels of $[Ca^{2+}]_o$ as in the corresponding experiments carried out without L-Phe. Specifically, WT, K47A, G146A, S169A and H413L were measured at 3.0 mM $[Ca^{2+}]_o$; Y63I and R415A were measured at 3.5 mM $[Ca^{2+}]_o$; I187A was measured at 10.0 mM $[Ca^{2+}]_o$; and W70L and I162A were measured at 12.5 mM $[Ca^{2+}]_o$. The average fluorescence intensity ratio at each increase in the level of $[Ca^{2+}]_o$ was plotted against $[Ca^{2+}]_o$ and fitted using the Hill equation, which gave EC$_{50}$ and Hill numbers. Values are means ± S.E.

Mutant	Starting Point (mM)		Frequency (Peaks/Min)		EC$_{50}$ (mM)		Hill Number	
	w/o L-Phe	w L-Phe	w/o L-Phe	w L-Phe	w/o L-Phe	w L-Phe	w/o L-Phe	w L-Phe
WT	3.0 ± 0.1	2.0 ± 0.2[b]	1.5 ± 0.1	2.2 ± 0.2[b]	2.9 ± 0.1	1.8 ± 0.2[b]	3.2 ± 0.3	4.1 ± 0.1[b]
K47A	2.4 ± 0.1[a]	1.9 ± 0.1[b]	1.6 ± 0.1	2.8 ± 0.2[b]	2.5 ± 0.1	1.7 ± 0.1[b]	3.0 ± 0.1	3.6 ± 0.2[b]
Y63I	3.3 ± 0.2	2.4 ± 0.2[b]	1.6 ± 0.2	2.0 ± 0.2[b]	2.8 ± 0.2	1.7 ± 0.1[b]	3.9 ± 0.1	3.6 ± 0.2[b]
W70L	13.9 ± 1.0[a]	9.2 ± 0.3[b]	2.7 ± 0.2	3.1 ± 0.2[b]	8.2 ± 0.3	7.8 ± 0.1	1.8 ± 0.1	3.7 ± 0.2[b]
G146A	2.5 ± 0.1[a]	1.9 ± 0.1[b]	2.0 ± 0.1	2.9 ± 0.2[b]	2.6 ± 0.1	1.9 ± 0.1[b]	2.5 ± 0.1	3.3 ± 0.1
I162A	13.0 ± 1.2[a]	9.6 ± 0.3[b]	1.4 ± 0.1	2.5 ± 0.2[b]	7.9 ± 0.4	11.3 ± 0.1	2.0 ± 0.1	1.5 ± 0.1
S169A	3.0 ± 0.2	2.3 ± 0.1[b]	1.6 ± 0.1	2.3 ± 0.2[b]	3.2 ± 0.2	2.2 ± 0.1[b]	3.3 ± 0.1	3.9 ± 0.1
I187A	8.1 ± 0.4[a]	3.4 ± 0.1[b]	1.8 ± 0.1	N/A	9.0 ± 0.3	3.4 ± 0.1[b]	1.6 ± 0.1	2.6 ± 0.1[b]
H413L	2.8 ± 0.2	1.4 ± 0.1[b]	1.3 ± 0.1	2.1 ± 0.1[b]	3.4 ± 0.2	2.1 ± 0.1[b]	3.4 ± 0.2	3.6 ± 0.1
R415A	3.5 ± 0.3	2.8 ± 0.2[b]	1.8 ± 0.2	2.6 ± 0.3[b]	3.0 ± 0.2	2.5 ± 0.1[b]	2.9 ± 0.2	3.4 ± 0.1[b]

[a] significant difference between mutant receptor and WT CaSR without L-Phe, $p < 0.05$; [b] significant difference between cases without L-Phe and with 5 mM L-Phe, $p < 0.05$
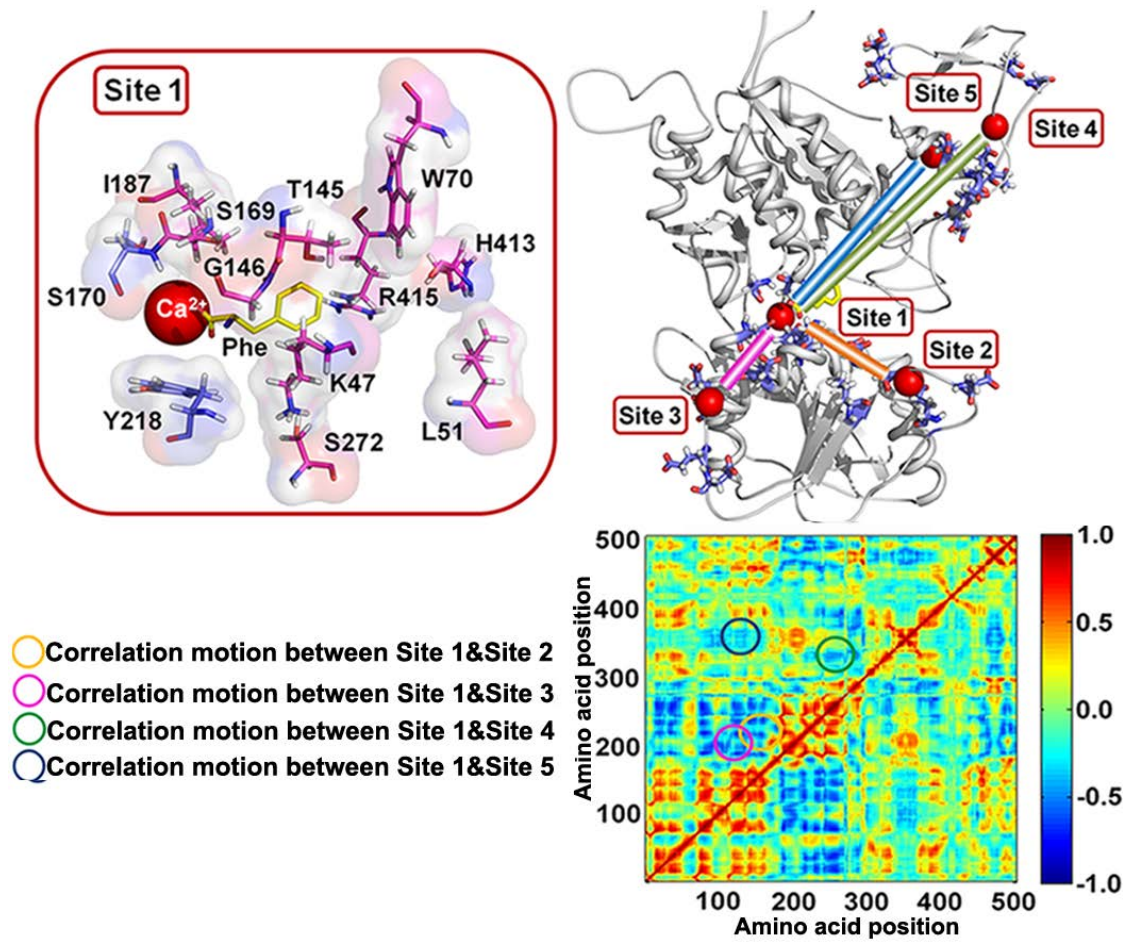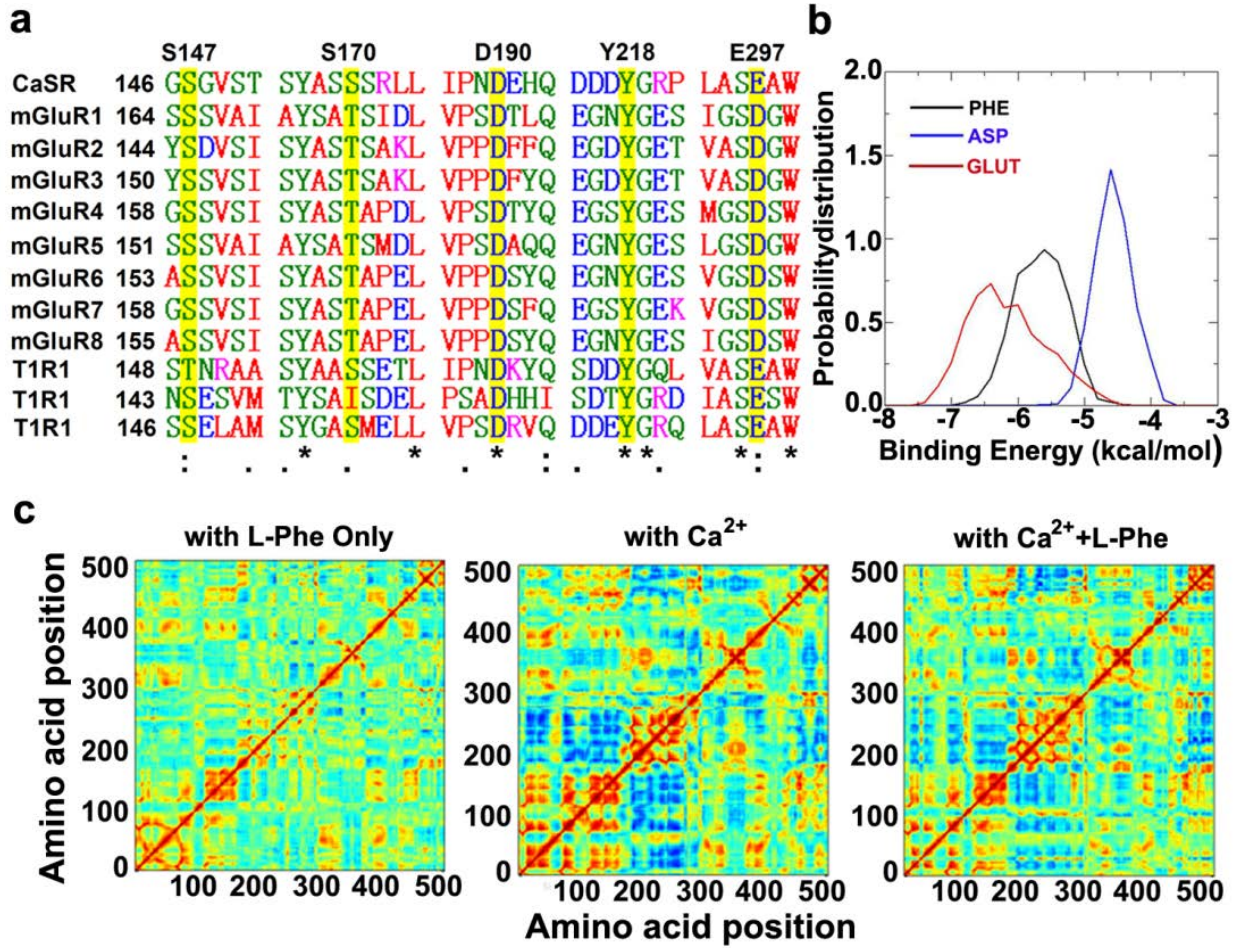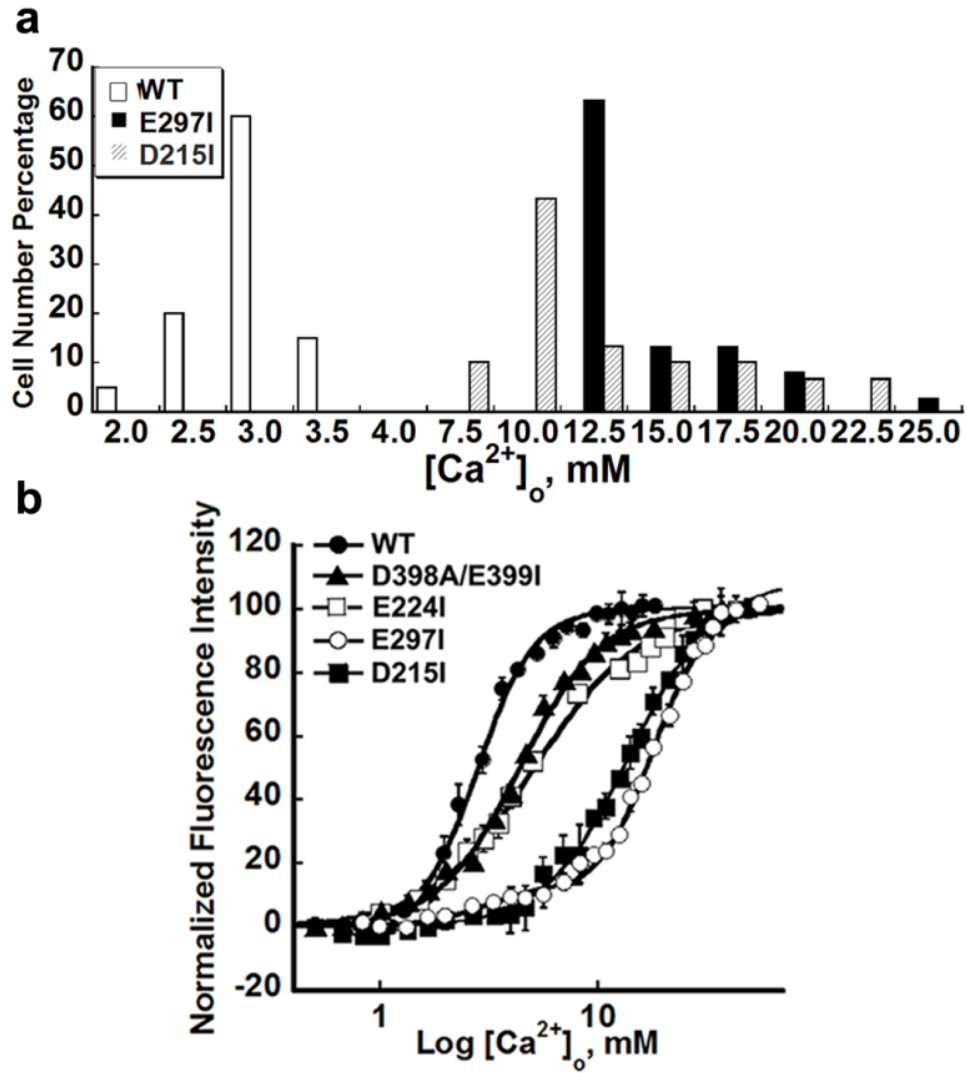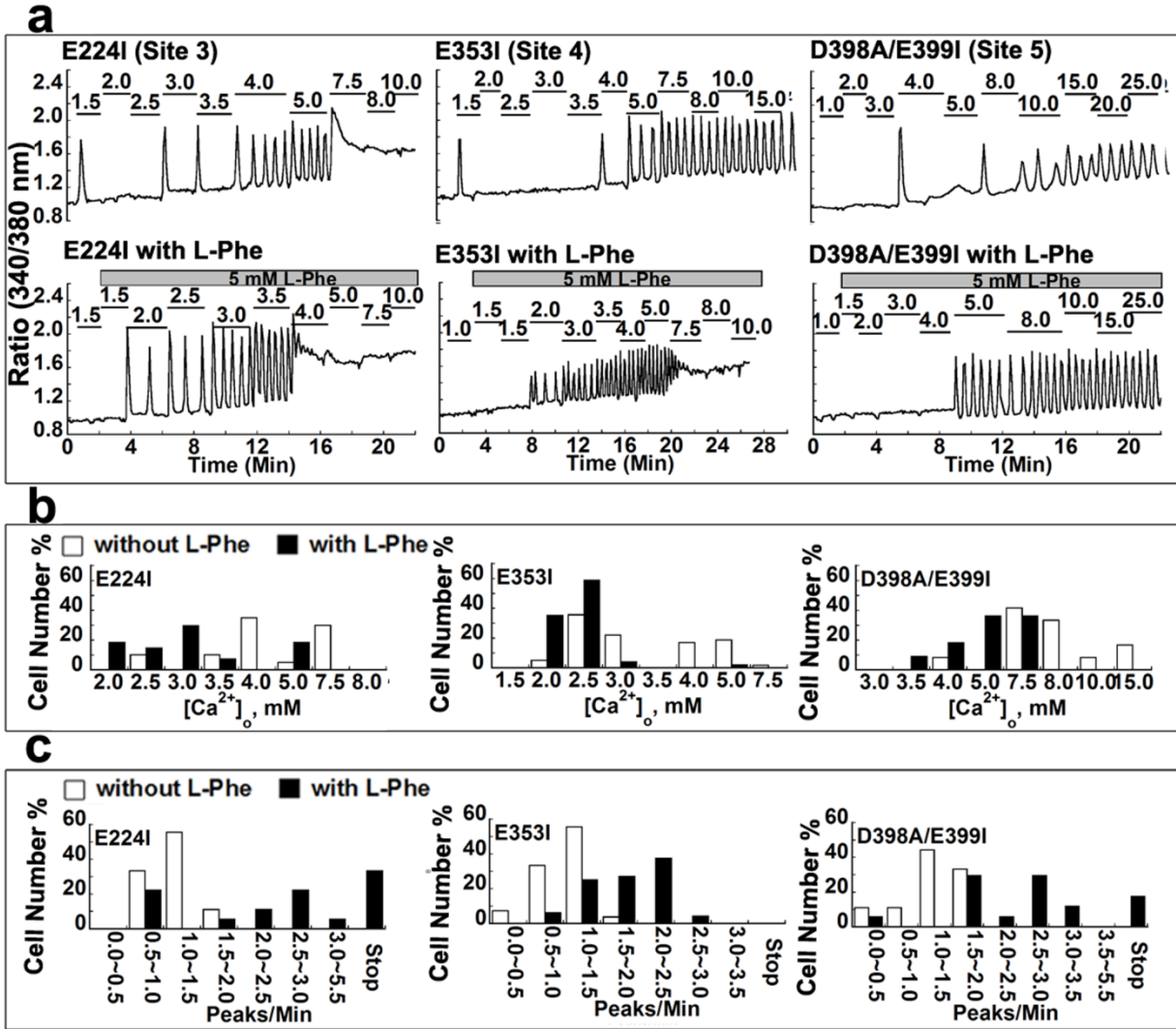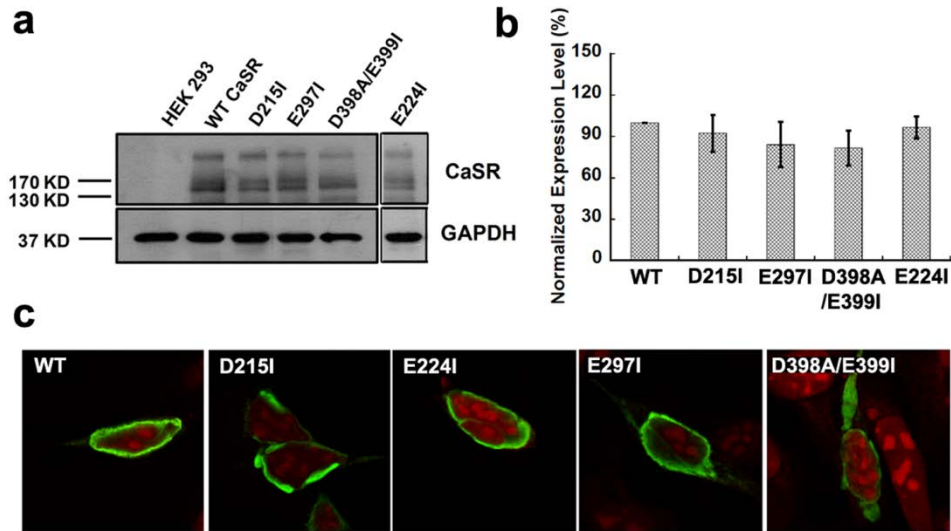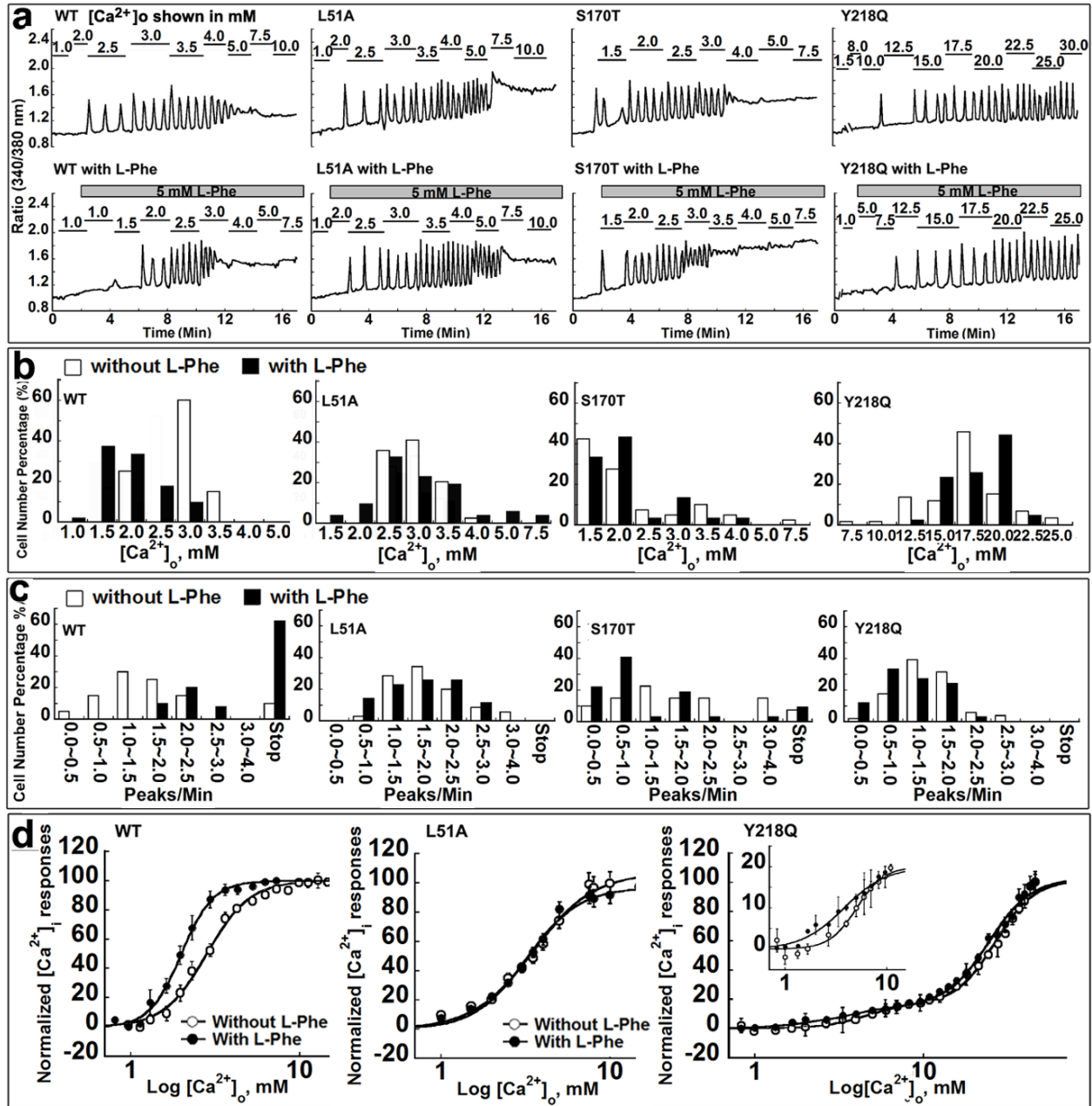
Figure 1

Figure 2
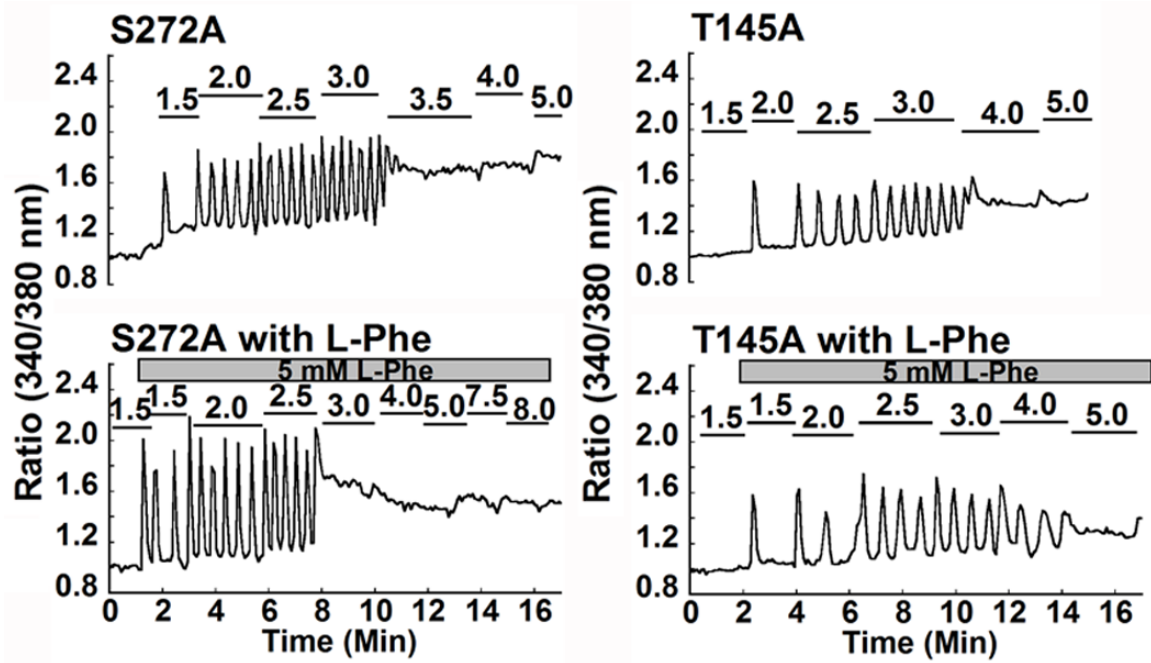
25

Figure 3

Figure 4

Figure 5

Figure 6

Figure 7

Figure 8
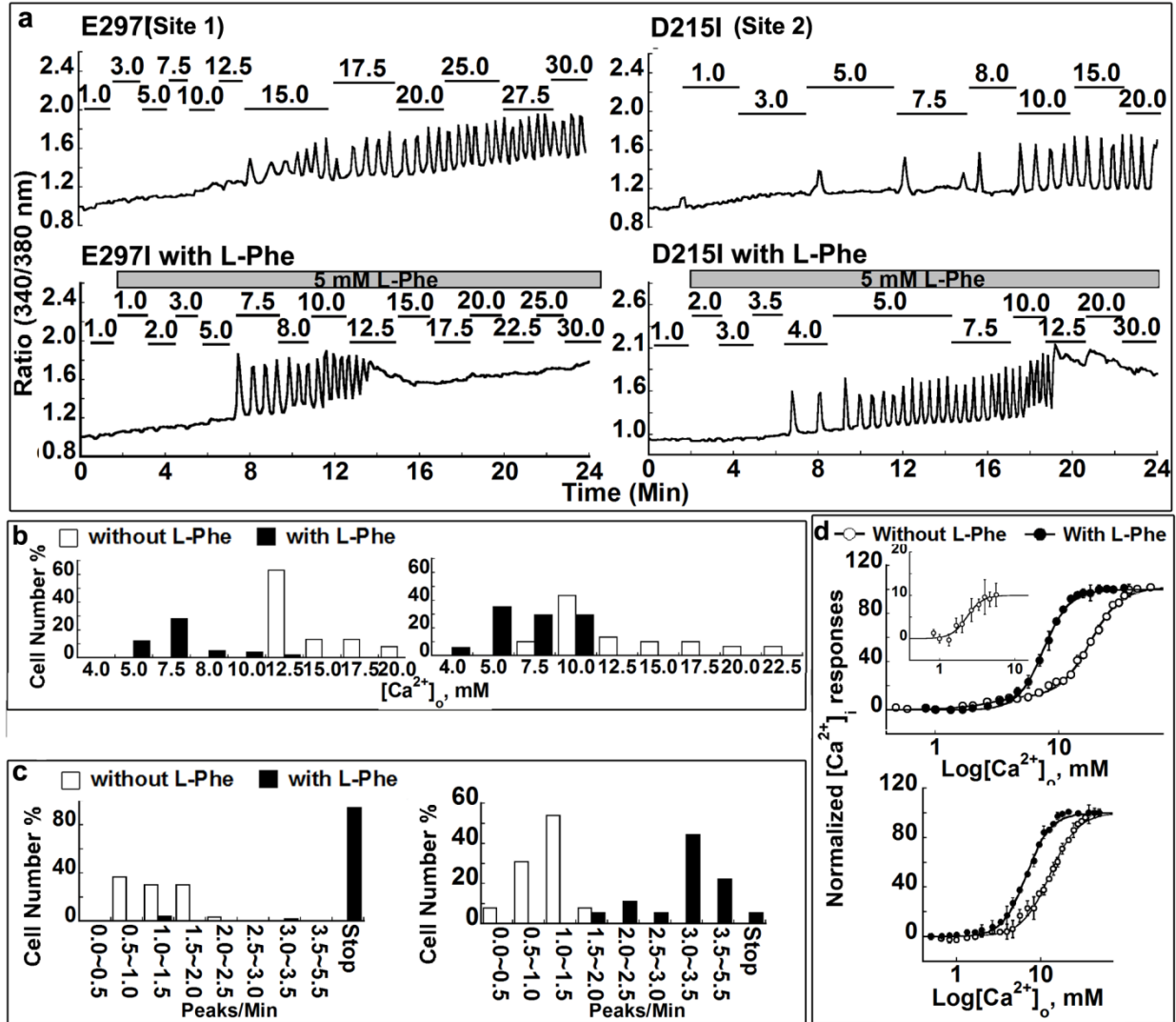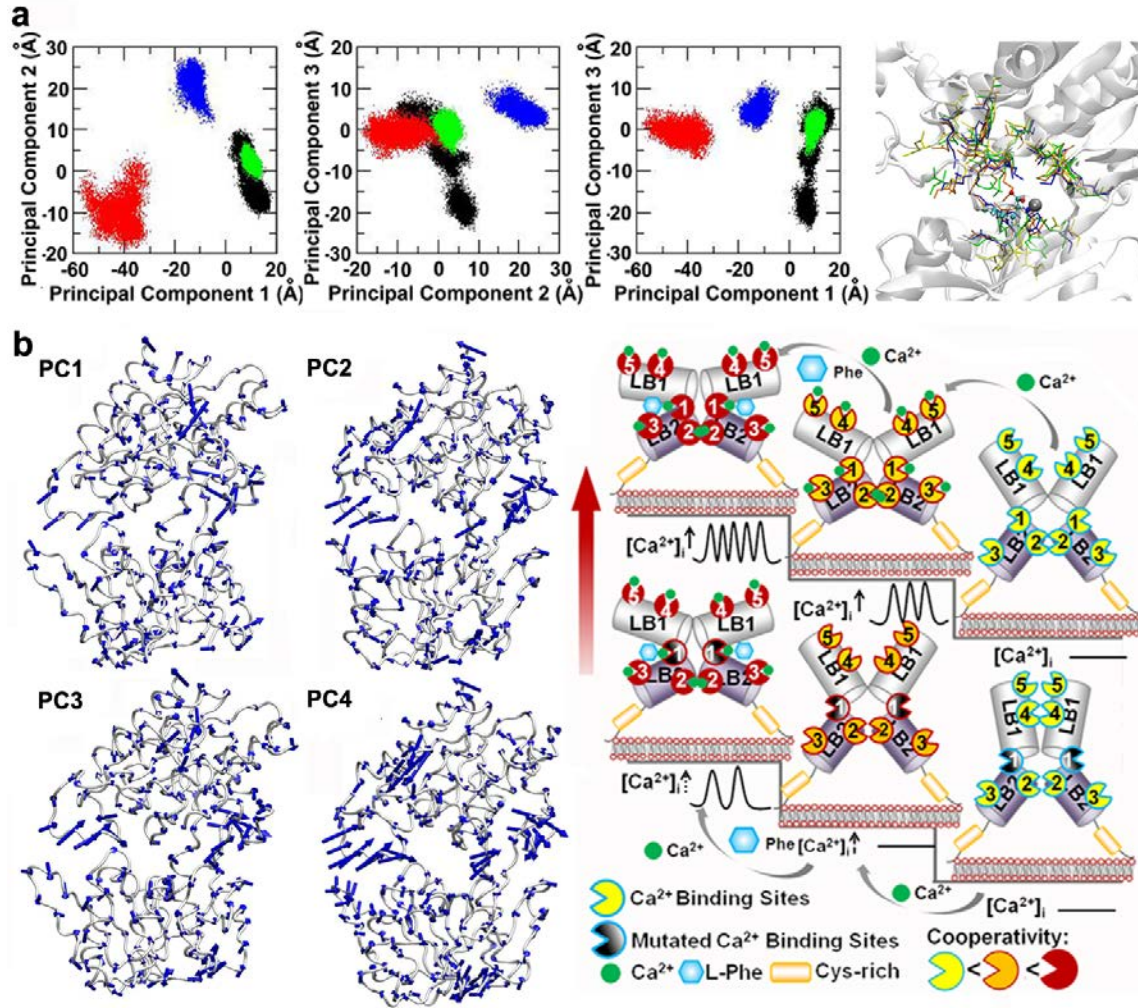
Figure 9

Identification of an L-Phenylalanine Binding Site Enhancing The Cooperative Responses of The Calcium Sensing Receptor to Calcium

Chen Zhang, Yun Huang, Yusheng Jiang, Nagaraju Mulpuri, Ling Wei, Donald Hamelberg, Edward M. Brown and Jenny J. Yang

Access the most updated version of this article at doi: 10.1074/jbc.M113.537357

Alerts:
- When this article is cited
- When a correction for this article is posted

Click here to choose from all of JBC's e-mail alerts

This article cites 0 references, 0 of which can be accessed free at
http://www.jbc.org/content/early/2014/01/06/jbc.M113.537357.full.html#ref-list-1